



Geological Analysis and Resource Assessment of Selected Hydrocarbon Systems

Deliverable

GARAH WP3 D3.3: Gas Hydrate overview report

Authors and affiliation:

Ricardo León Buendía, IGME

Christopher Rochelle, BGS

Margaret Stewart, BGS

André Burnol, BRGM

Tove Nielsen, GEUS

John Hopper, GEUS

Julia Giménez, IGME

Isabel Reguera, IGME

Silvia Cervel, IGME

Pilar Mata, IGME

E-mail of lead author:

r.leon@igme.es

Version: 22-09-2021

This report is part of a project that has received funding from the European Union's Horizon 2020 research and innovation programme under grant agreement number 731166.





Deliverable Data		
Deliverable number	D3.3	
Dissemination level	Public	
Deliverable name	GARAH WP3 D3.3: Gas hydrate overview report	
Work package	WP3, Addressing knowledge gaps in hydrate assessment in the European continental margin	
Lead WP/Deliverable beneficiary	IGME	
Deliverable status		
Submitted (Author(s))	31/05/2021	Ricardo León Buendia, IGME Christopher Rochelle, BGS Margaret Stewart, BGS André Burnol, BRGM Tove Nielsen, GEUS John Hopper, GEUS Julia Giménez, IGME Isabel Reguera, IGME Silvia Cervel, IGME Pilar Mata, IGME.
Verified (WP leader)	22/09/2021	Ricardo León, IGME
Approved (Coordinator)	23/09/2021	Niels Hemmingsen Schovsbo, GEUS



GENERAL INTRODUCTION

The aim of Geological Analysis and Resource Assessment of Selected Hydrocarbon Systems (GARAHS) is to develop a harmonized, science-based geological analysis and assessment of conventional and unconventional hydrocarbon resources that will help member states continue the transition to lower carbon energy sources. This will contribute to climate commitments and allow planning for secure sources of affordable energy. The analysis and assessment of hydrocarbons will focus on two areas:

(i) A geological analysis and resource assessment of petroleum systems in Europe's major petroleum province, the North Sea. This research includes the assessment of conventional and unconventional oil and gas resources in the most important hydrocarbon basin in Europe. This will enable the remaining resources to be better understood and managed and will identify options for multiple and alternative uses of the subsurface as producing fields come off-line.

(ii) An assessment of hydrates on the European continental margin and related risks from a pan-European viewpoint. The assessment of gas-hydrate resources on the European continental margin fills an information gap of pan-European interest. This will improve the understanding of the potential role that gas hydrates may play in the future EU energy mix, as it will constitute a baseline for future projects aimed at improving the European model of the gas hydrate stability zone (GHSZ), related hazards and potential for geological storage of CO₂.

A catalogue evaluating the multiple-use of hydrocarbon reservoirs as an integrated or alternative use of the subsurface, together with an appraisal of risks and safety, will also be produced.



Abstract

This report presents the current state of hydrate-related data in the European continental margins and analyses it in order to define critical knowledge gaps and areas of interest for future joint projects and for assessing the potential of CO₂-rich hydrates for safe geological storage and hydrate-related geohazards and risks. Hydrate-related data show a heterogeneous distribution and knowledge gaps (areas with <1 records per 100 km²) have been defined. Some of these knowledge gaps have been classified as critical: east of Greenland, Svalbard, the northern Norwegian margin, the southern-western Barents Sea and the White Sea, the north of the British Islands, the Gulf of Cádiz, the Bay of Biscay, the north-western Iberian margin and the south Mediterranean Sea. For a fully interoperability of the hydrate related information, future hydrate related data should be collected and stored compliant the data model structure of the hydrate GIS-data base of GARAH project. Nine areas of interest for future scientific projects were defined based on the critical knowledge gaps, potential CO₂ storage and geohazard risk: east Greenland and Svalbard, the west Barents and White seas, the northwest Norwegian margin, the northwest British Islands, the Bay of Biscay and the northwest Iberian margin, the southern Iberian and northern Moroccan margins, the Tunisian and Libyan margins, the eastern Mediterranean, and the Black and Marmara seas. The Bay of Biscay shows a potential safe CO₂ deep offshore storage capacity: 3,422 km³ and 3,700 km³, in the French and Spanish EEZ, respectively. Finally, the susceptibility assessment of occurrence of hydrate dissociation processes on the seafloor shows high values in Svalbard, the northern Norwegian margin—Barents Sea, the continental slope of the mid-Norwegian margin and the North Sea, the Gulf of Cádiz and the eastern Mediterranean and the Black Sea. Moderate values are observed on the continental shelf of western Greenland, the northwest of the British Islands and the continental slope of the western and northern Mediterranean Sea.



TABLE OF CONTENTS

1. INTRODUCTION.....	6
1.1. Objectives.....	6
1.2. Scope and framework.....	6
2. CURRENT STATE OF HYDRATE-RELATED PAN-EUROPEAN DATA	8
2.1. Geological and geophysical data.....	8
2.2. Oceanographic data and environmental constraints.....	15
3. CRITICAL DATA GAPS IN HYDRATE ASSESSMENT	20
3.1. The geothermal gradient	21
3.2. Seafloor temperature.....	23
3.3. Bathymetry	25
3.4. Sediment thickness	28
3.5. Ocean production and sediment rate.....	29
4. AREAS OF INTEREST FOR FUTURE SCIENTIFIC PROJECTS	33
5. POTENTIAL SAFE GEOLOGICAL STORAGE OF CO ₂ AS MIXED GAS HYDRATES.....	38
5.1. The “deep offshore” CO ₂ storage as mixed gas hydrates.....	39
5.2. Potential safe CO ₂ deep offshore storage capacity in the French and Spanish EEZs.....	41
5.1. Conclusions and perspectives	43
6. HYDRATE-RELATED GEOHAZARDS	44
6.1. Susceptibility map assessment of seafloor areas affected by hydrate dissociation.....	44
6.1. Discussion	52
7. CONCLUSIONS.....	53
8. REFERENCES.....	54



1. INTRODUCTION

1.1. Objectives

The main objective of the report (D3.3) is to integrate and analyse all the results obtained in the previous tasks: (3A) collection of hydrate-related data and (3B) development of a hydrate-related GIS database.

This report shows the current state of marine methane hydrate-related pan-European data in a harmonized GIS model in order to (i) identify critical knowledge gaps, (ii) provide information on areas of interest for future joint projects, (iii) assess the potential of CO₂-rich hydrates for safe geological storage, and (iv) assess related geohazards and risks.

1.2. Scope and framework

The study area of the present report involves the geographical area of the European Marine Observatory Data Network (EMODnet) Bathymetry (Fig. 1.1 A). The geographical limits for identifying critical knowledge gaps and areas of interest for future joint projects and for assessing the potential of CO₂-rich hydrates for safe geological storage and hydrate-related geohazards and risks are therefore 30°W to 43°E and 25°N to 85°N.

However, because hydrate data for the neighbouring area were stored in the databases collected in this project (PERGAMON, MIGRATE and EMODnet), we extended the GIS database to western Greenland (Fig. 1.1 B) and the Barents Sea (Fig. 1.1 C).

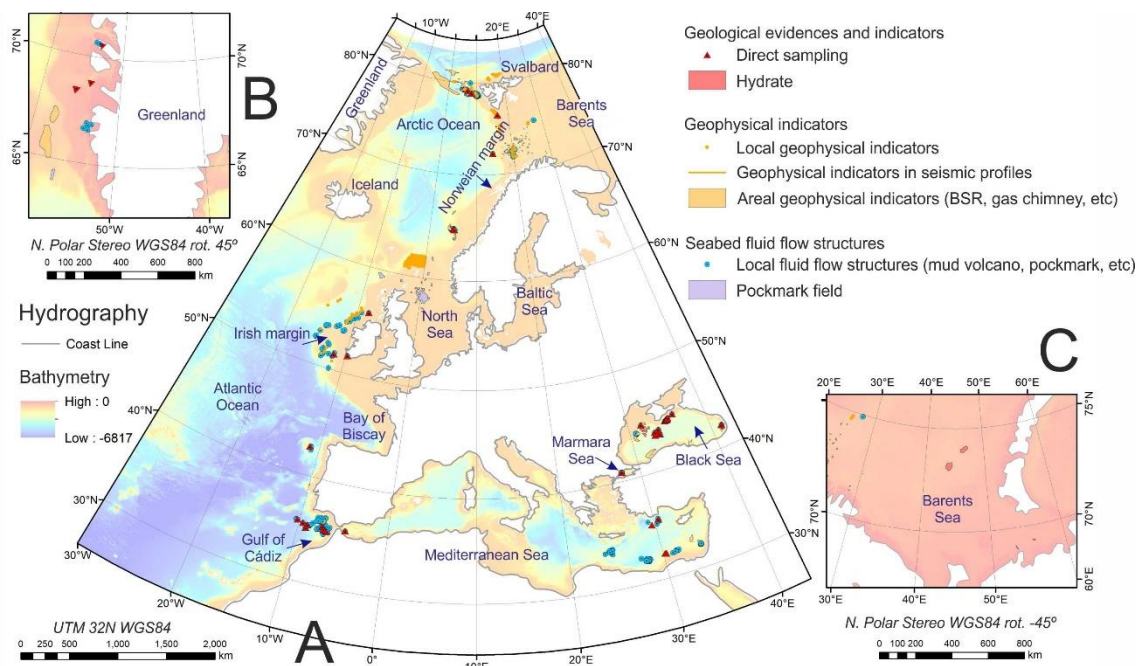


Fig. 1.1. Study area of GARAH WP3



This report presents the current state of hydrate-related pan-European data (Section 2). Available data were also analysed in order to identify critical data gaps for understanding gas hydrates along the European continental margins (ECMs) (Section 3). Based on the results of the knowledge gap assessment, the selected areas with low density or lack of data are assessed in order to establish priority areas for future projects (Section 4). An application of the gas hydrate-related GIS database presented is shown in the assessment of (i) CO₂-rich hydrates for the safe geological storage of CO₂ (Section 5) and (ii) hydrate-related geohazards (Section 6).

The hydrate-related risk was assessed in order to determine the impact of possible destabilization of hydrates on the seafloor and the potential links with geohazards. The risk analysis was addressed in the scope of the susceptibility assessment. The likelihood of the seafloor being affected by natural and human-induced hydrate dissociation processes was also considered.

Finally, an overview of the main highlights of WP3 is presented in Section 8.



2. CURRENT STATE OF HYDRATE-RELATED PAN-EUROPEAN DATA

The current state of hydrate-related pan-European data was grouped for assessment into two sets of geological/geophysical and oceanographic data: (i) data of a pan-European scope from free public databases such as EMODnet, PERGAMON and MIGRATE; and (ii) data of a regional scope from scientific organizations (GEUS, IGME, BGS, BRGM, NOC and CAGE, among others).

2.1. Geological and geophysical data

The geological and geophysical data focused on marine methane hydrate evidence and indicators. The term hydrate evidence refers to hydrate samples recovered by direct sampling (gravity core, dredge, etc), while the term hydrate indicators refers to indirect signs of the presence of hydrates in the seafloor or sediment column based on geophysical or geochemical anomalies. They were reported along the ECMs of Greenland and Svalbard, the Norwegian margin, the northern British Islands, the southern Iberian and northwest African margins (Gulf of Cádiz and Alborán Sea), the Black Sea, the Marmara Sea and the eastern Mediterranean Sea (Fig. 2.1).

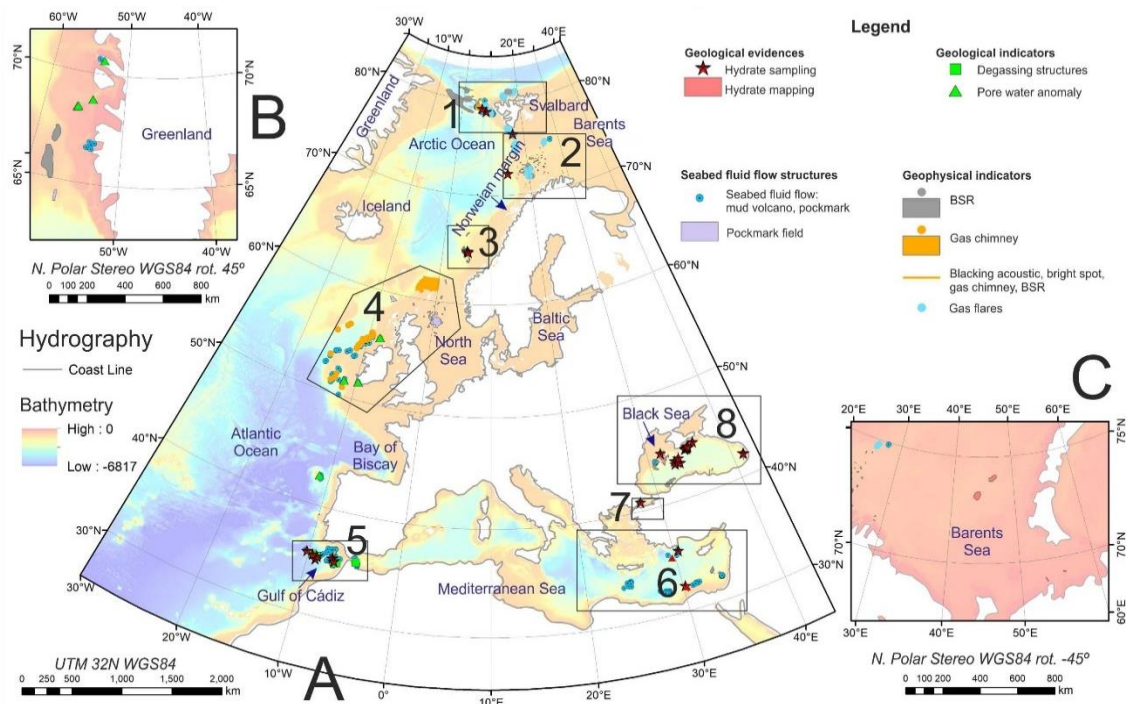


Fig. 2.1. Evidence and indicators of hydrates on the European continental margins stored in the GARAH GIS hydrate database. **A.** Study area (EMODnet Bathymetry area). 1, Svalbard; 2, Svalbard-Barents-Norwegian margins; 3, mid-Norwegian margin; 4, offshore northern British Islands; 5, southern Iberian and northwest African margins; 6, eastern Mediterranean Sea; 7, Marmara Sea; 8, Black Sea. Bathymetry source EMODnet Bathymetry. **B.** Indicators offshore of west Greenland. Bathymetry sourced from IBCAO. **C.** Evidence in the Barents Sea. Bathymetry sourced from IBCAO.



The Arctic Ocean groups the evidence and indicators of offshore Greenland, Svalbard, the northern Norwegian margin and the Barents Sea: in particular, 10 direct hydrate samples (hydrate evidence) and ca. 2160 km² of hydrate mapping, 223 geophysical hydrate indicators (of which 38,836 km² correspond to bottom-simulating reflectors [BSRs] and gas chimneys) and more than one thousand individual gas seepages.

The majority of indicators of offshore Greenland are BSR levels (Fig. 2.2). Locally, on the west margin, individual seepages have been observed and pore water anomalies have been recovered in gravity cores. The source is thermogenic gas migrating through faults and fractures (Mikkelsen et al., 2012; Hopper et al., 2014; Nielsen et al., 2011, 2014).

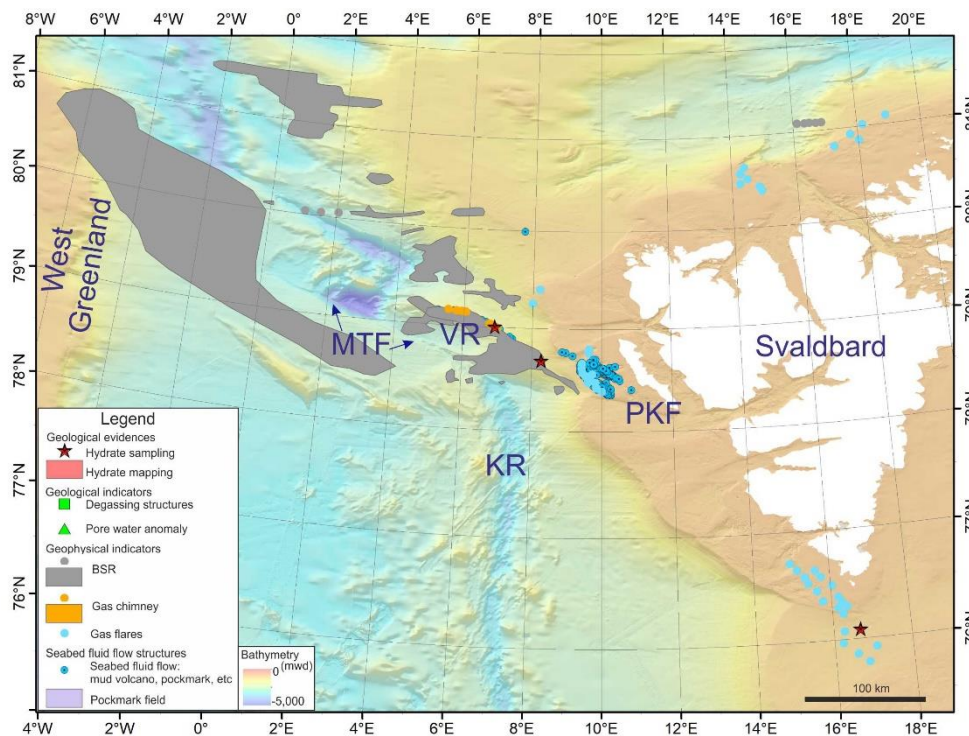


Fig. 2.2. Evidence and indicators of hydrates in offshore Svalbard and west Greenland. VR, Vestnesa Ridge; PKF, Prinz Karl Forland; MTF, Molloy Transform Fault; KR, Knipovich Ridge.

Offshore of Svalbard, hydrate evidence and indicators have been collected at two locations: the Vestnesa Ridge and Prinz Karl Forland (Fig. 2.2). Direct evidence is represented by three recovered samples of gas hydrates. A total of 81 seismic indicators have been collected: in the water column mainly gas flares (68) and in the sediment column gas chimneys, seismic blanking, bright spots and BSRs (ca. 8,000 km²). In the vicinity of these indicators, ca. 1,000 pockmarks and seepages have been reported. The gases are dominantly of thermogenic origin in Svalbard, migrating through faults (Plaza-Faverola et al., 2015), with a



microbial contribution at Prinz Karl Forland (Plaza-Faverola et al., 2017; Smith et al., 2014). Abiotic methane was inferred in the western zone of the South Molloy Transform Fault and the west Knipovich Ridge region (Johnson et al., 2015; Waghorn et al., 2018). A volume of 700 km³ was estimated from BSRs and the theoretical GHSZ.

The south Svalbard–Barents–northern Norwegian margins constitute a widespread region with a great deal of hydrate evidence and indicators (Fig. 2.3). The main hydrate region has been reported in the southern Barents Sea, with 2,163 km² mapped (Fig. 2.1 C; Petrov et al., 2019). On the other side, two local cases of direct evidence have been reported in the Håkon-Mosby mud volcano (Vogt et al., 1997; Ginsburg et al., 1999) and one in the Storfjordrenna region (Serov et al., 2017). Seventeen seabed fluid flow structures (pockmarks, hydrate pingos and mud volcanoes) directly related to the hydrates have been reported. More than 150 geophysical indicators have been reported on the south Svalbard–Barents–northern Norwegian margins. Forty-six of them are local BSRs, bright spots and gas flares detected on seismic profiles; the rest are mapped surfaces of BSR levels and gas chimneys (a total of 3,876 km²). The gases are mostly thermogenic, migrating through faults and fractures. Finally, the volume is estimated to be 0.19 GSm³ in Bjørnøya Basin (Laberg et al., 1998) and 93–650 GSm³ (Vadakkepuliyambatta et al., 2017) or 470–3320 GSm³ (Minshull et al., 2020) in the southwest Barents Sea.

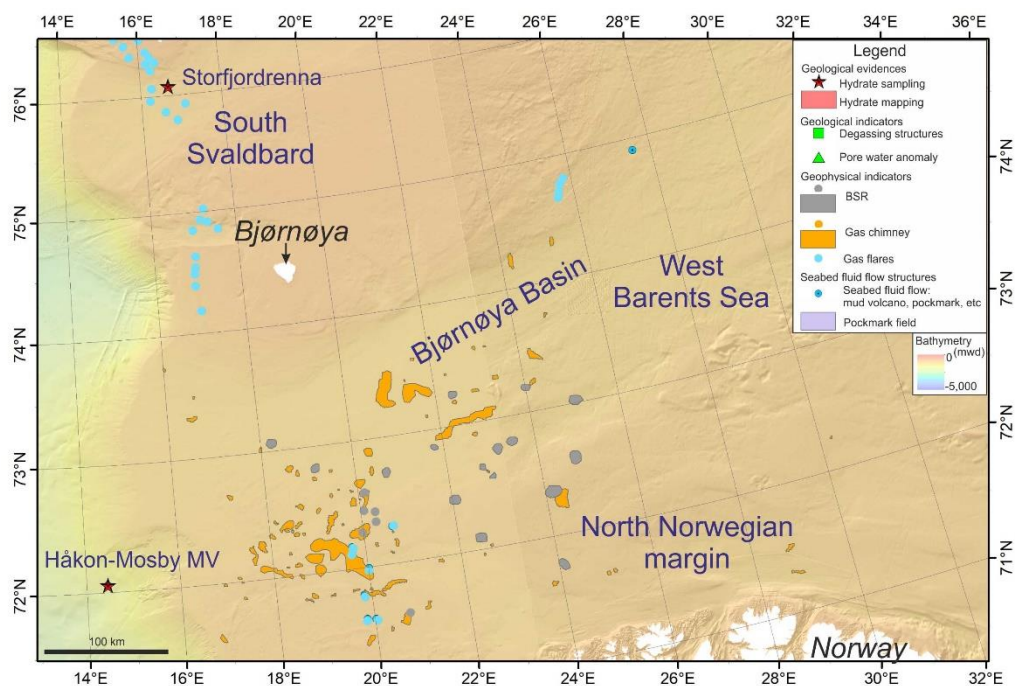


Fig. 2.3. Evidence and indicators of hydrates on the south Svalbard–Barents–northern Norwegian margins

The Atlantic Ocean is the largest part of the study area. Evidence and indicators have been reported on the mid-Norwegian, Irish and southern Iberian



and northwest African margins. However, direct hydrate evidence has only been recovered on the mid-Norwegian margin and in the Gulf of Cádiz (Fig. 2.1).

On the mid-Norwegian margin (“3” in Fig. 2.1), hydrate evidence and indicators are mostly circumscribed to the vicinity of the eastern and northern flanks of the head of the Storegga Slide (Fig. 2.4). The direct hydrate evidence was collected from six gravity cores during the TTR-16 cruise (Akhmetzhanov et al., 2008). Approximately 4,300 km² of BSRs have been mapped along the north flank of the Storegga Slide (Bugge et al., 1988; Posewang and Mienert 1999; Bouriak et al., 2000; Bünz et al., 2003), together with pockmarks and other seismic indicators such as bright spots and gas chimneys. The gases have a primarily microbial origin but with a significant thermogenic component (Vaular et al., 2010). The total volume of gas in this area (both hydrate and free gas zones) has been estimated at 625 GSm³ (Senger et al., 2010).

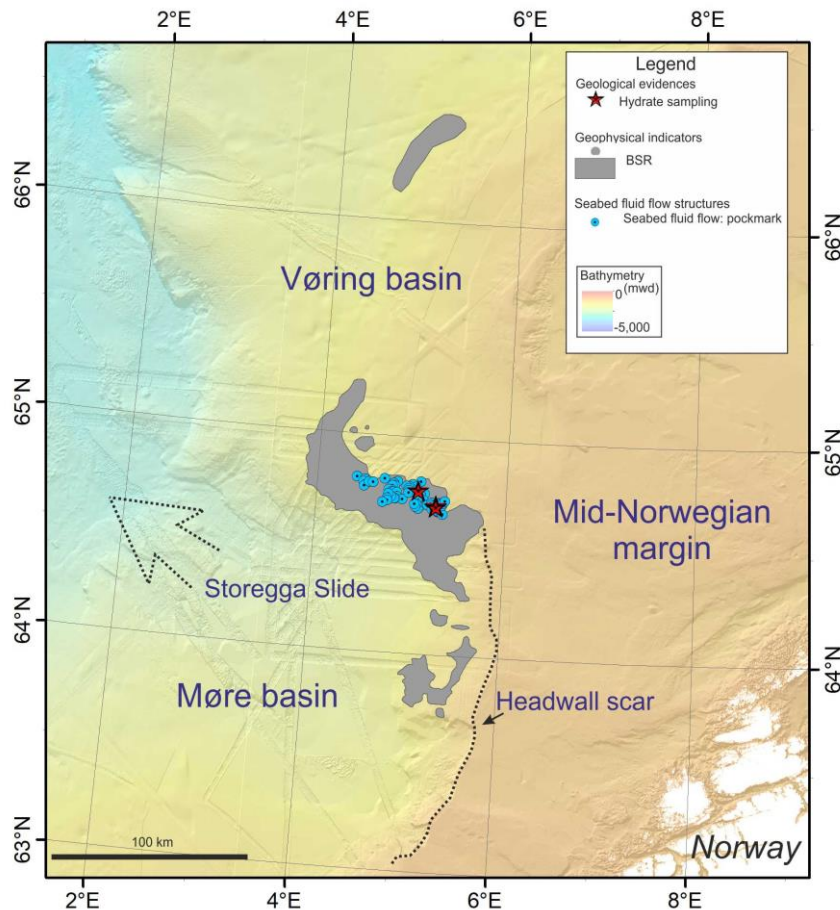


Fig. 2.4. Evidence and indicators of hydrates on the mid-Norwegian margin

Although hydrates have not been detected offshore of Ireland and northern Scotland, several seabed fluid flow structures and hydrate indicators have been observed in close proximity to the theoretical GHSZ base of the HSZ (Fig. 2.5) (Roy et al., 2018; Minshull et al 2020). The indicators are pore water anomalies



(Irish margin) and seismic amplitude anomalies such as bright spots, seismic gas pipes and chimneys, blacking acoustic facies and BSRs.

Offshore of the southern Iberian and northwest African margins, hydrate evidence and indicators have been detected only in association with mud volcanoes. Direct samples of hydrates (25) were recovered in the Gulf of Cádiz, first during the TTR programme (Kenyon et al., 2000, 2001, 2002, 2006, 2006; Akhmetzhanov et al., 2007, 2008; Ivanov et al., 2010) and later during several scientific cruises (Kopf et al 2004; Hensen et al., 2015). The indicators in cores are mainly degassing structures and pore water anomalies and those in seismic profiles are seismic amplitude anomalies such as bright spots, seismic gas pipes and chimneys, blacking acoustic facies and BSRs (Depreiter et al., 2005; León et al., 2006). Seabed fluid flow structures such as mud volcanoes, pockmarks, collapses and authigenic carbonates have been recovered in the vicinity of this evidence (Somoza et al., 2003; Diaz-del-Rio et al., 2003; León et al., 2006, 2010, 2012; Magalhaes et al., 2012) (Fig. 2.6). Hydrate and hydrocarbon gases sampled from mud volcano sediments include both microbial and thermogenic components (Mazurenko et al., 2002; Stadnitskaia et al., 2006).

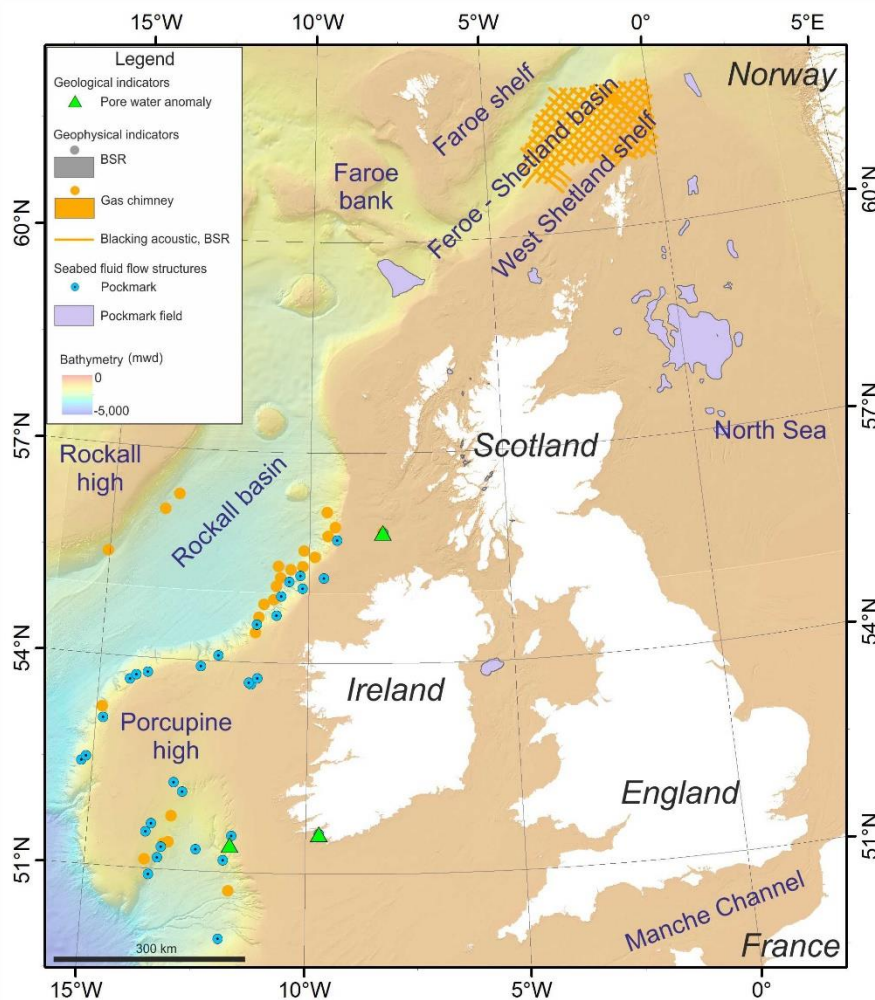


Fig. 2.5. Hydrate indicators offshore of the northern British Islands

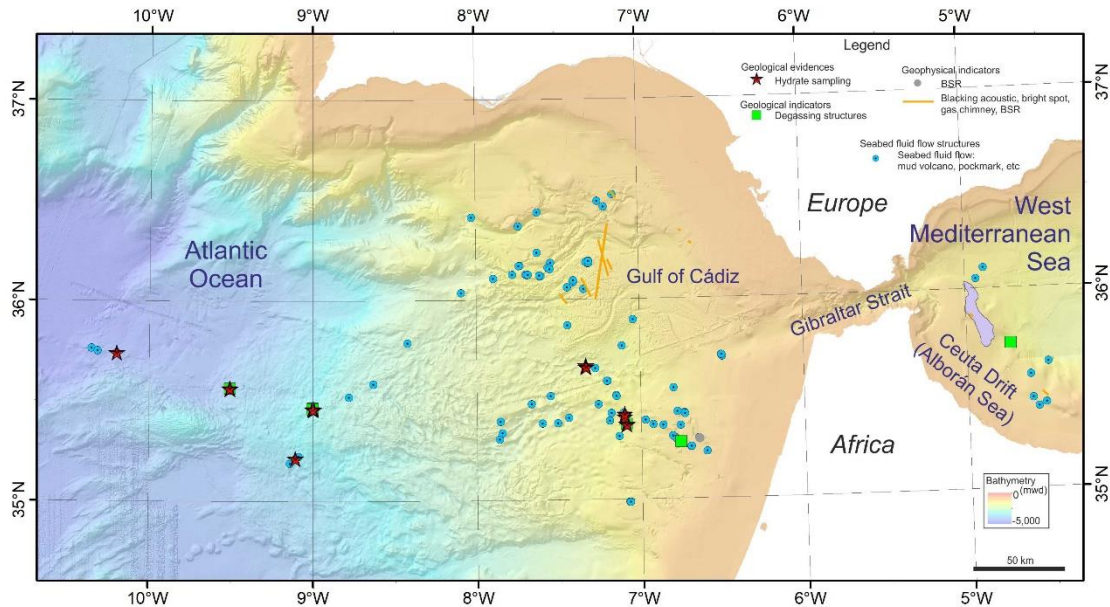


Fig. 2.6. Hydrate indicators on the southern Iberian and northwest African margins

In the eastern Mediterranean and Marmara seas, direct samples of hydrates have been recovered in both mud volcanoes (Woodside et al., 1997; Lykousis et al., 2009; Aloisi et al., 2000) and mounts (the Western High in the Marmara Sea; Bourry et al., 2009). Furthermore, indicators such as a soupy texture (Lykousis et al., 2009) and their signatures in pore water chlorinity and chemistry (de Lange and Brumsack, 1998a; Pape et al., 2010) have also been reported. At Milano MV, $5 \times 10^9 \text{m}^3$ of methane as hydrate and free gas has been estimated (De Lange and Brumsack, 1998b). Offshore of Israel, about $2,500 \text{ km}^2$ of BSR levels have been mapped (Fig. 2.7). Many focused seepages such as mud volcanoes and pockmarks (about 600 sites) are present. In particular, numerous mud volcanoes are present, primarily along the accretionary complex and to a lesser extent on the Nile fan (Masclé et al., 2014; Zitter et al., 2005), showing clear thermogenic signatures (Pape et al., 2010). Gas seepage features include gas bubbling, pockmarks and authigenic carbonates at the seafloor, and a variety of seismic reflection anomalies beneath the seabed, including bright spots and seismic blanking with a microbial methane gas signal (Römer et al., 2014).

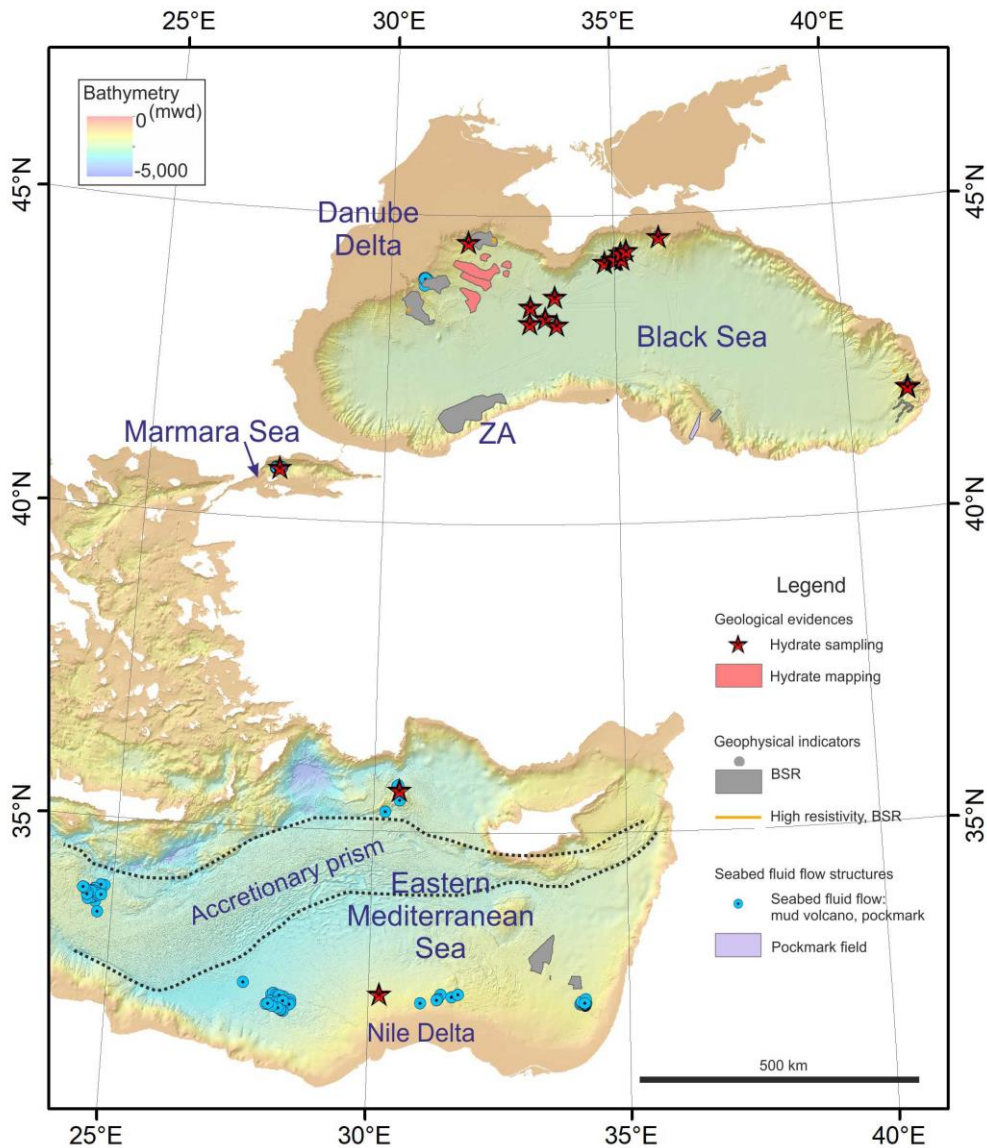


Fig. 2.7. Hydrate evidence and indicators in the western Mediterranean, Marmara and Black seas. ZA, Zonguldak-Amasra.

In the Black Sea, 23 cases of gas hydrate evidence (Yefremova and Zhizchenko 1974; Riboulot et al., 2018) and ca. 3,700 km² of seafloor mapped as hydrates (Popescu et al., 2007; Zander et al., 2017) have been reported. More than 3000 gas plumes in the water column have been detected (Egorov et al., 2011), the majority of them marking the present-day upper limit of the GHSZ. At some sites, such as offshore of the Danube delta, the hydrate is of microbial origin and is related to periodic seabed anoxia conditions. At other sites, such as offshore of Zonguldak-Amasra, thermogenic gases are found, in addition to microbial gas in the shallow sediments.



2.2. Oceanographic data and environmental constraints

Hydrate-related oceanographic data were focused on the oceanographic continuous variables controlling the GHSZ, such as seafloor temperature, geothermal gradient and bathymetry (pressure). Sediment thickness was also considered an environmental constraint.

Seafloor Temperature is a dataset developed in Task 3C in the Spanish Geological Survey using CTD (conductivity, temperature and depth) data. The CTD data originate from the World Ocean Database (<https://www.ncei.noaa.gov/products/world-ocean-database>) and were downloaded with ODV (<https://odv.awi.de/>) on 2019-05-27T13-05-21. The CTD/STD cast data were provided by the British Oceanographic Data Centre (<https://www.bodc.ac.uk/>). The final map was created by picking the last temperature record of the CTD or STD sounder if it reached the seafloor (Fig. 2.8).

Geothermal Gradient is a dataset from the global heat flow database of the International Heat Flow Commission (website: <http://engineering.und.edu/geology-and-geological-engineering/globe-heat-flow-database/index.cfm>). The data were downloaded with the ODV application (<https://odv.awi.de/>) (Fig. 2.9).

The bathymetry dataset is composed of two sets: EMODnet Bathymetry and IBCAO. EMODnet Bathymetry is a free public dataset (<https://www.emodnet-bathymetry.eu/>) that covers the study area of WP3 of the GARAH project. IBCAO (https://www.gebco.net/data_and_products/gridded_bathymetry_data/arctic_ocean/) is also a free public dataset and was added in order to supply a bathymetric base map for the hydrate evidence and indicators located outside the limits of EMODnet Bathymetry, such as those for west Greenland and the southern Barents Sea (Fig. 2.10).

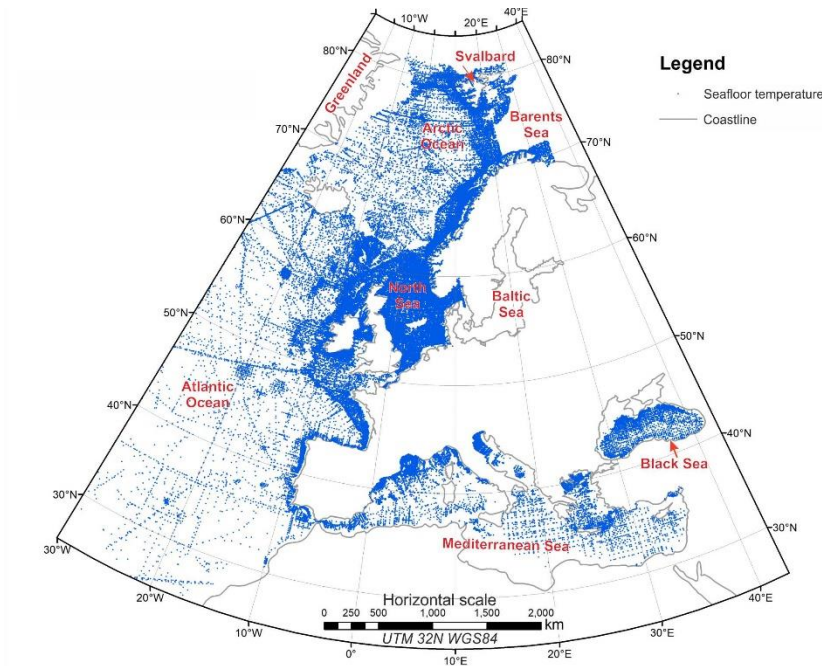


Fig. 2.8. Location of the CTD data considered in the Seafloor Temperature dataset.

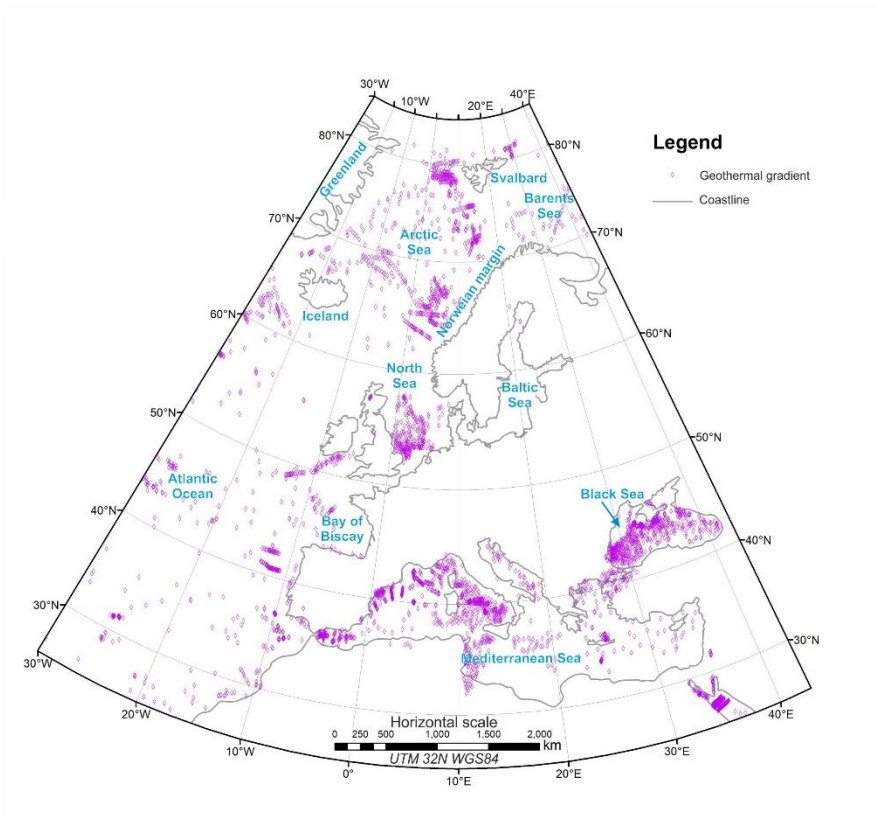


Fig. 2.9. Location of the Geothermal Gradient records.

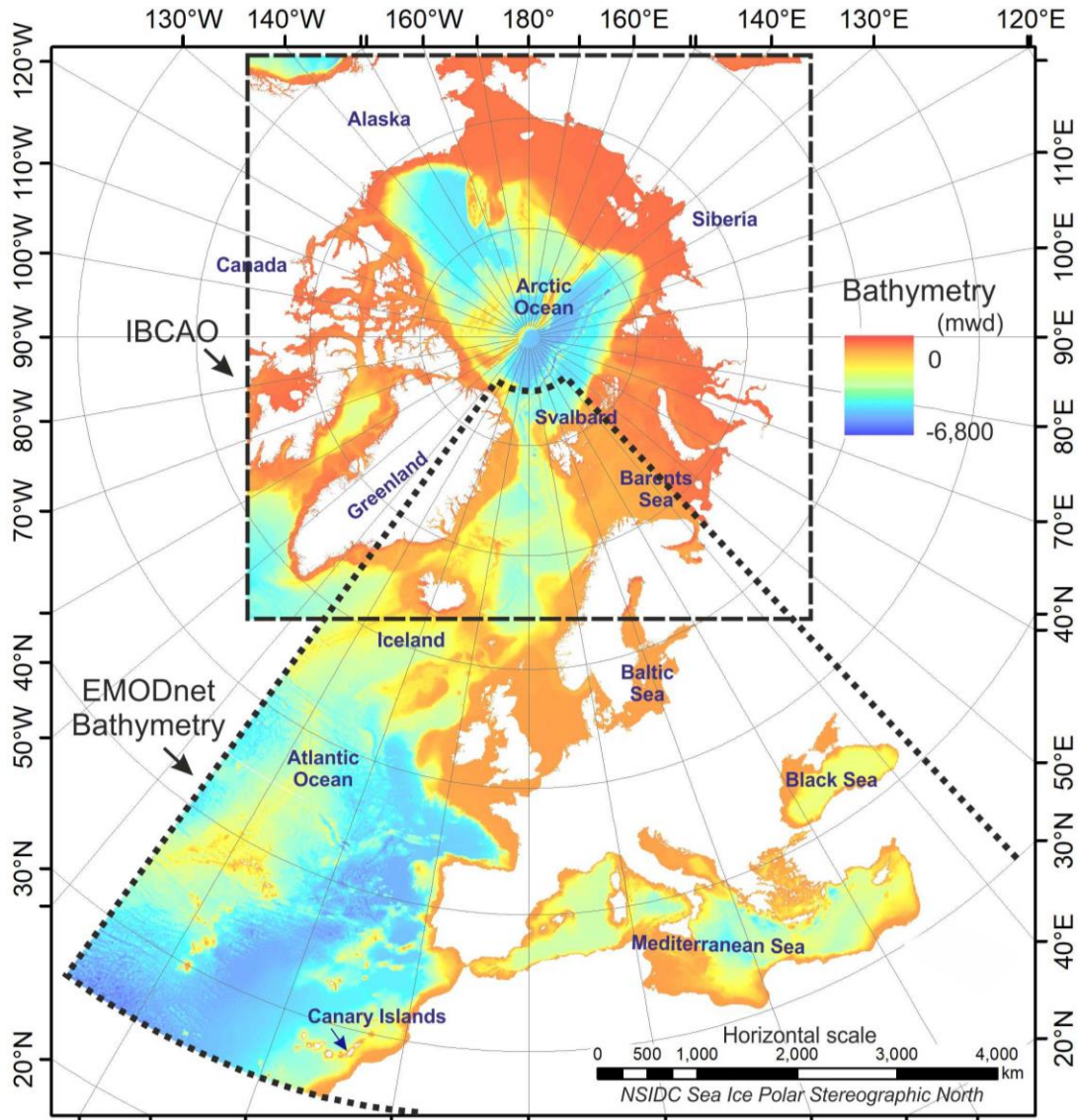


Fig. 2.10. The bathymetry dataset used in WP3 of the GARAH project.

The sediment thickness dataset was added in order to supply a geological constraint for the theoretical hydrate or GHSZ thickness. It is a raster dataset containing the total sediment thickness of the world's oceans and marginal seas. Data were collected from the National Oceanic and Atmospheric Administration (query 27/09/2019; <https://data.noaa.gov/dataset/dataset/total-sediment-thickness-of-the-worlds-oceans-marginal-seas-version-2>) (Fig. 2.11).

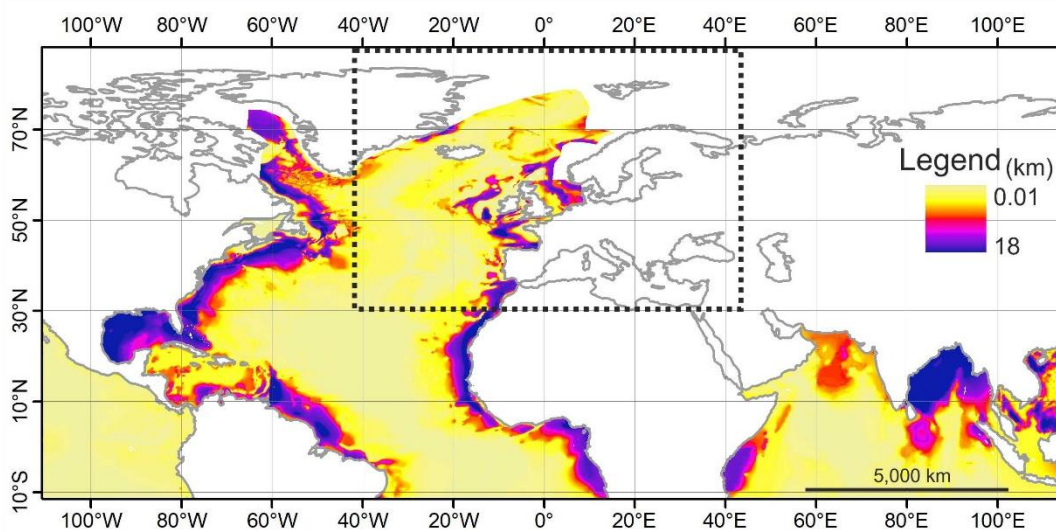


Fig. 2.11. Global sediment thickness. Black dotted line, study area.

Sediment rate is a key parameter for the conversion of organic material into gas hydrate. A sediment dataset was therefore added from the free pan-European public portal of EMODnet Geology (Fig. 2.12; https://www.emodnet-geology.eu/map-viewer/?bmagic=y&baslay=baseMapEEA,baseMapGEUS&optlay=&extent=-2179400,-295790,7283560,5318790&layers=emodnet_sediment_accumulation_rates).

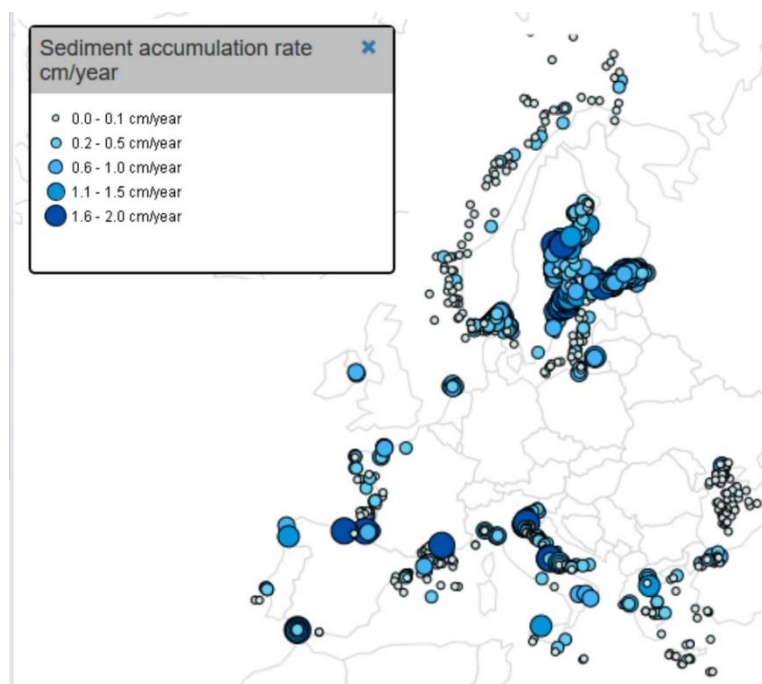


Fig. 2.12. Records of sedimentation rate along continental margins. Source, EMODnet Geology (<https://www.emodnet-geology.eu/>).



Finally, a layer related to ocean production was added in order to supply an information dataset related to the organic material production in the oceans. This model stores the photosynthetic rates ($\text{g C m}^{-2} \text{yr}^{-1}$) derived from satellite-based chlorophyll concentrations (<http://sites.science.oregonstate.edu/ocean.productivity/standard.product.php>).

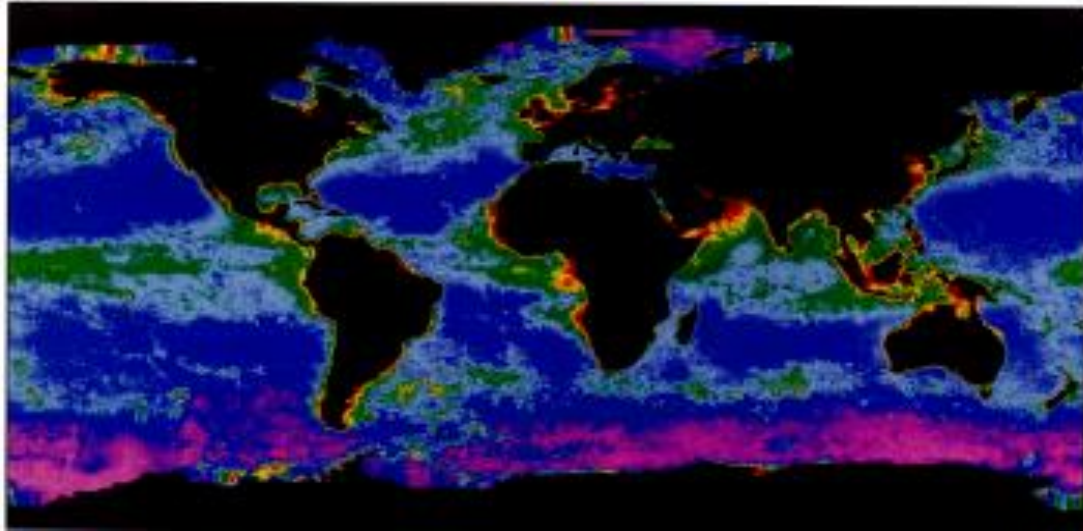


Fig. 2.13. Global estimates of annual phytoplankton primary production using the vertically generalized production model V(GPM).

3. CRITICAL DATA GAPS IN HYDRATE ASSESSMENT

Evidences of marine methane hydrates have been reported in eight main regions along the ECMs (Fig. 3.1): offshore of Greenland, Svalbard, the Norwegian margin, offshore of the northern British Islands, the southern Iberian and northwest African margins (the Gulf of Cádiz and the Alborán Sea), the Black Sea, the Marmara Sea and the eastern Mediterranean.

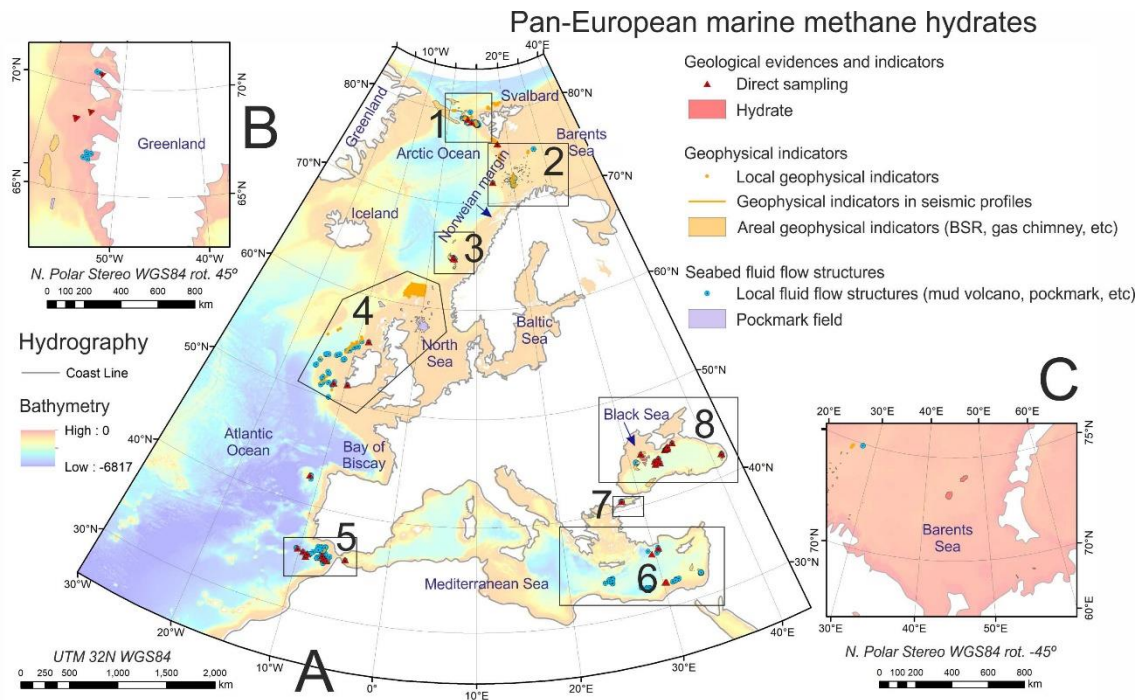


Fig. 3.1. Evidence and indicators of hydrates on the European continental margins stored in the GARAH GIS hydrate database. **A.** Evidence in the EMODnet area (study area). 1, Svalbard; 2, western Barents Sea; 3, mid-Norwegian margin; 4, offshore of the northern British Islands; 5, offshore of the southern Iberian and northwest African margins; 6, eastern Mediterranean Sea; 7, Marmara Sea; 8, Black Sea. Bathymetry source, EMODnet Bathymetry. **B.** Evidence offshore of western Greenland. Bathymetry source, IBCAO. **C.** Evidence in the Barents Sea. Bathymetry source, IBCAO.

Nucleation and dissociation of marine methane hydrates are directly controlled by four environmental parameters: seafloor temperature, geothermal gradient, salinity and pressure (water depth) (Sloan, 2003). However, free public information about these key parameters for understanding the GHSZ shows a non-homogeneous continuity along the ECMs. This issue is especially important for giving a predictive (and quick) static and continuous model for the hydrate stability field along the whole of the ECMs.

Identifying the critical knowledge gaps provides (i) information on areas of interest for future joint projects; and (ii) the groundwork for future projects aimed at improving models of the GHSZ along the European margins.



Although several regional GHSZ models have been reported along the ECMs (Betlem et al., 2019; León et al., 2009; Roy et al., 2017; Wallmann et al., 2012), there is no pan-European model with a standardized methodology, unified quality of data, and an error and/or uncertainty prediction assessment. Such a model is essential for assessments relating to geohazards and risks, the abundance of sediment-hosted gas hydrates, and the role of CO₂-rich hydrates for the geological storage of CO₂. It is also of broad interest for the scientific community: petroleum geologists, biologists and ecologists working on vulnerable ecosystems, researchers on natural hazards and tsunamis, civil engineers and policy makers.

3.1. The geothermal gradient

Marine geothermal data show a heterogeneous distribution that is especially concentrated in areas surveyed by scientific cruises. However, this concentration appears only in some of the eight above-mentioned regions with hydrate evidence (Fig. 3.2).

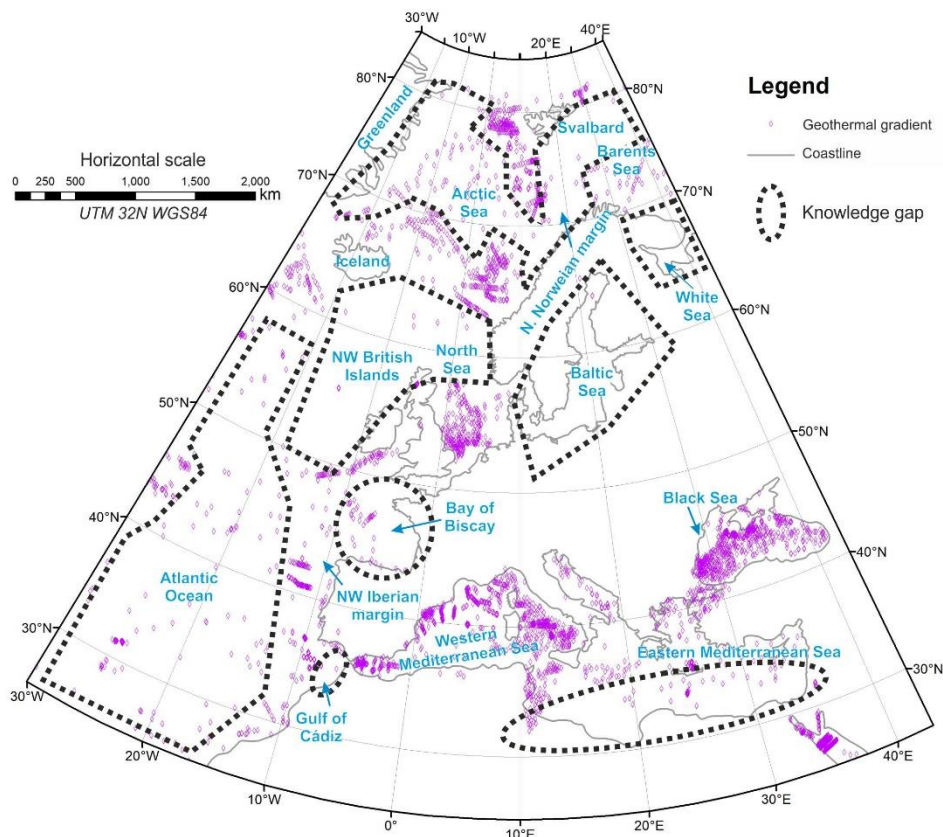


Fig. 3.2. Distribution of geothermal gradient data in the study area. Black dotted line, knowledge gap.



We selected as the geothermal gradient knowledge gap all seafloor areas with a low density of records of geothermal gradient. A density map of geothermal gradient data was developed using the kernel density algorithm of ArcGIS® with the following parameters: search radius, 5.64 km; area units, square kilometres; output values, densities; method, planar. Results are number of records per 100 km² (Fig. 3.3).

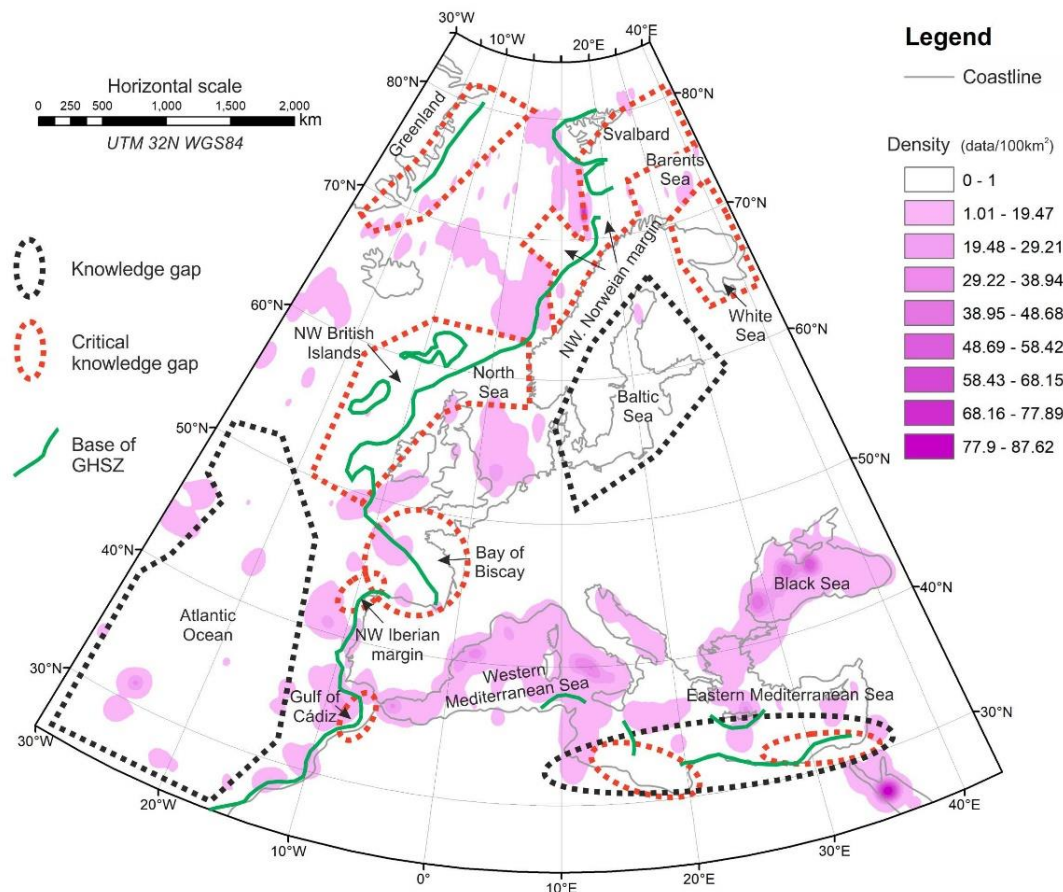


Fig. 3.3. Density map of geothermal gradient developed using the kernel density algorithm of ArcGIS®. Density in number of records per km². Black dotted line, knowledge gap. Red dotted line, critical knowledge gap.

On this map, the selected geothermal gradient knowledge gaps match with areas of zero or less than 1 record of geothermal gradient per 100 km².

These knowledge gaps are especially critical (i) in areas where direct samples of hydrates have been collected; (ii) in the vicinity of the base of the GHSZ; and (iii) in areas where seabed fluid flow structures have been detected. Taking into account these three scenarios, the knowledge gaps were classified as critical in the east of Greenland, Svalbard, the northern Norwegian margin, the southern Barents Sea and the White Sea, north of the British Islands, the Gulf of Cádiz, the Bay of Biscay, the northwest Iberian margin and the southwest Mediterranean Sea.



- In Svalbard, the northern Norwegian margin, the North Sea, north of the British Islands and the Gulf of Cádiz, because of the proximity of the base of the GHSZ and the presence of evidence and indicators of hydrates and seabed fluid flow structures.
- In the Bay of Biscay and the northwest Iberian margin, because of the proximity of the base of the GHSZ and the presence of seabed fluid flow structures.
- In the southwestern Mediterranean Sea, because of the lack of information, the presence of seabed fluid flow structures and the proximity of the base of the GHSZ.
- In the east of Greenland, because of the lack of information and the proximity of the base of the GHSZ.
- In the southern Barents Sea and the White Sea, because of the lack of information and the presence of evidence and indicators of hydrates.

Finally, the hydrate scientific community has a critical need to understand the geothermal gradient and to gather more data, especially better data coverage overall. In particular, in areas having a relatively high spatial variance in the geothermal gradient, a high-resolution coverage is critical in order to assess the potential for uncertainty predictions for similar areas with no data.

3.2. Seafloor temperature

Marine methane hydrates are stable under low-temperature conditions (Sloan, 2003). Seafloor temperature is the most sensitive variable in the theoretical calculation of the base of the GHSZ (Burnol et al., 2015; León et al., 2009). Data collected in the GARAH project show a heterogeneous distribution (Fig. 3.4). The Black Sea and the eastern Atlantic continental shelf are the areas of greatest concentration of seafloor temperature data in the ECMs. Nevertheless, areas with lack of information have been observed and are classified as *seafloor temperature knowledge gap areas*: east of Greenland, the western Barents Sea, the Baltic Sea, the northern Black Sea, the northern mid-Atlantic Ocean, the deep Bay of Biscay, the southern Gulf of Cádiz and the southeastern Mediterranean Sea (black dot lines in Fig. 3.4).

A density map of seafloor temperature data was developed using the kernel density algorithm of ArcGIS® with the following parameters: search radius, 5.64 km; area units, square kilometres; output values, densities; method, planar. The results are the number of records per 100 km² (Fig. 3.5).

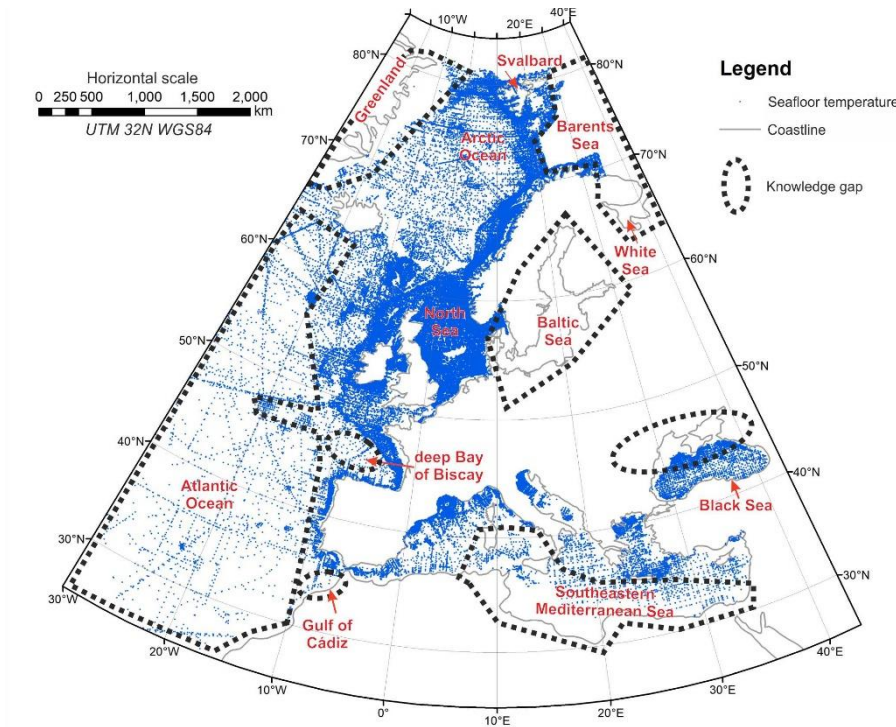


Fig. 3.4. Distribution of seafloor temperature data in the study area. Black dotted line, knowledge gap.

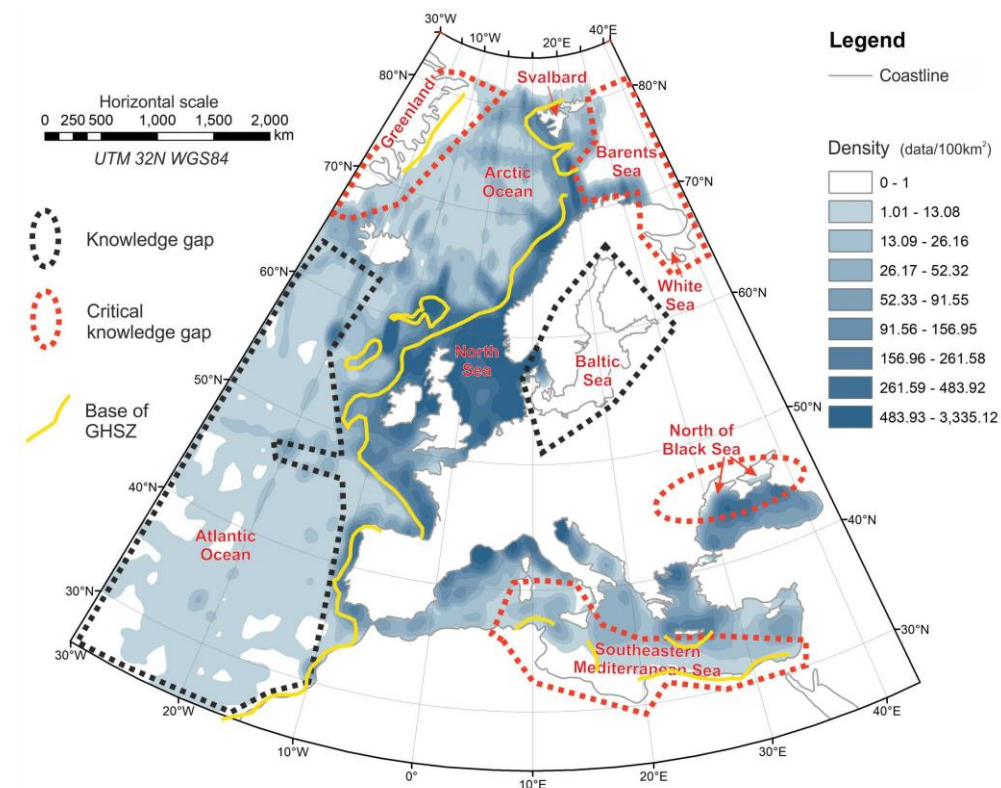


Fig. 3.5. Density map of seafloor temperature data developed using the kernel density algorithm of ArcGIS®. Density in number of records per km². Black dotted line, knowledge gap. Red dotted line, critical knowledge gap.



On this map, the selected geothermal gradient knowledge gaps match with areas of less than 1 measure of seafloor temperature per 100 km².

As stated in the geothermal gradient section (section 3.1), these knowledge gaps are especially critical (i) in areas where direct hydrate sampling has been performed; (ii) in the vicinity of the base of the GHSZ; and (iii) in areas where seabed fluid flow structures have been detected. Taking into account these three scenarios, the following *critical seafloor temperature knowledge gaps* were identified: east of Greenland, the western Barents Sea and White Sea, the northern Black Sea and the southeastern Mediterranean Sea.

- East of Greenland, because of the lack of information and the proximity of the base of the GHSZ.
- In the western Barents Sea and White Sea, because of the lack of information and the proximity of evidence and indicators of hydrates.
- In the northern Black Sea and southeastern Mediterranean Sea, because of the lack of information, the proximity of evidence of hydrates and the presence of seabed fluid flow structures.

3.3. Bathymetry

Marine methane hydrates are stable under high pressure (water depth) conditions (Sloan, 2003). On the ECMs, the base of the GHSZ ranges widely from zero in the Arctic region to 400-500 mwd at low European latitudes (Betlem et al., 2019; León et al., 2009; Roy et al., 2017; Wallmann et al., 2012).

In general, the public bathymetry data collected (EMODnet Bathymetry and IBCAO) are of quite acceptable quality and have been very useful for the objectives of this hydrate-related pan-European study. Although the whole study area is covered by bathymetry data (there are no gaps in bathymetry information) at a resolution of 1/16 arc minutes (ca. 115 m grid), differences in accuracy can be observed regionally (e.g. between the northwest European margin, Fig. 3.6, and the southern Mediterranean Sea, Fig. 3.7).

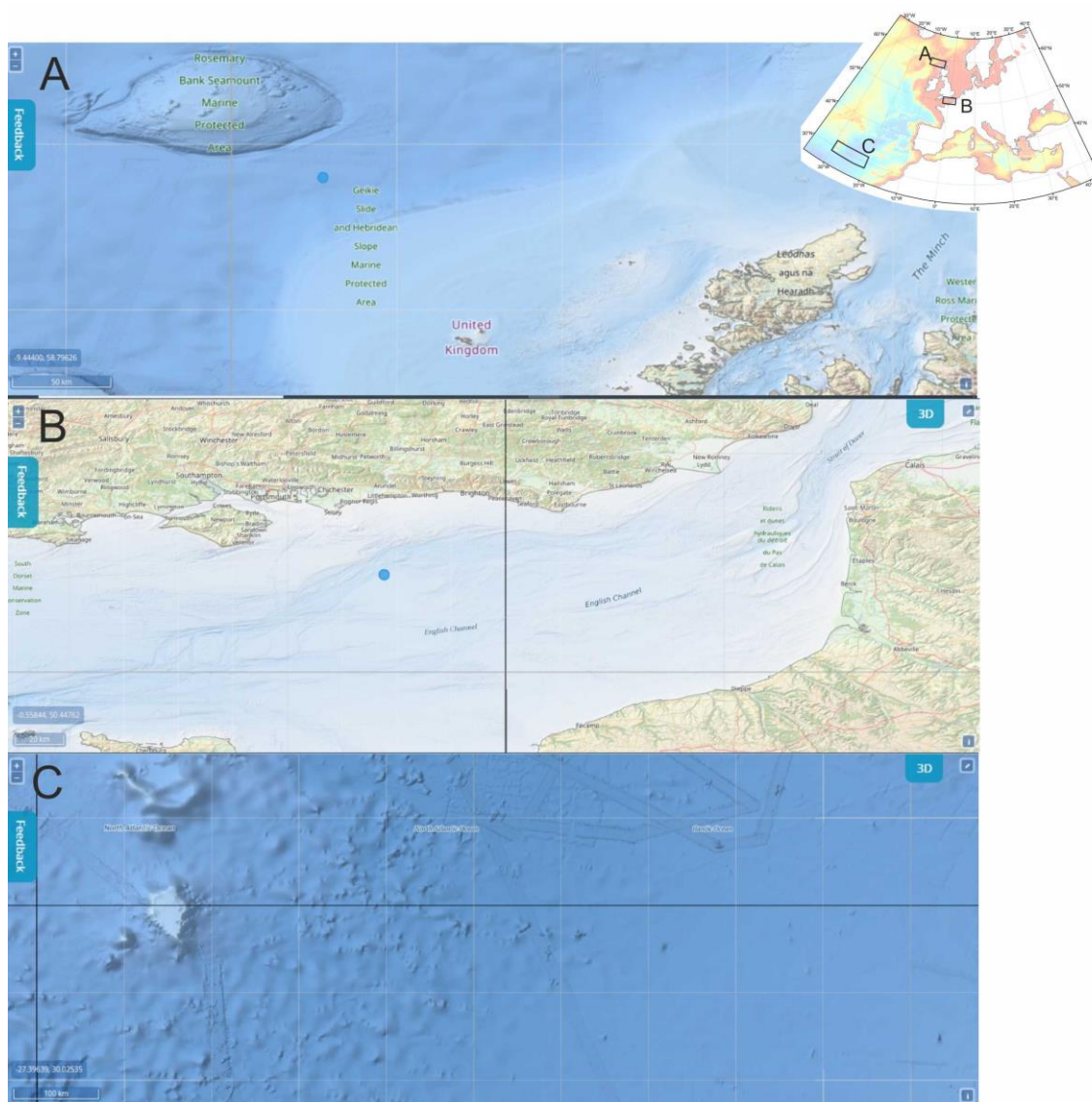


Fig. 3.6. Bathymetry models of the Atlantic area. A. Northern Irish margin. B. Scottish margin. C. English Channel. D. Atlantic Ocean. Source, EMODnet Bathymetry (<https://portal.emodnet-bathymetry.eu/>).

The EMODnet Bathymetry dataset has a quality index for the bathymetry datum calculated for each pixel. This quality index is calculated from the statistical parameters of the bathymetry measures on which the final value for each pixel is calculated: the minimum water depth in metres to the lowest astronomical tide (LAT), the average water depth in metres to the LAT, the maximum water depth in metres to the LAT, the standard deviation of water depth in metres, the number of values used for interpolation over the grid cell, the interpolation flag (identification of extrapolated cells), the average water depth smoothed by means of a spline function in metres to the LAT, an indicator of the offsets between the average and smoothed water depth as a percentage of the water depth, and a reference to the prevailing source of data with metadata.

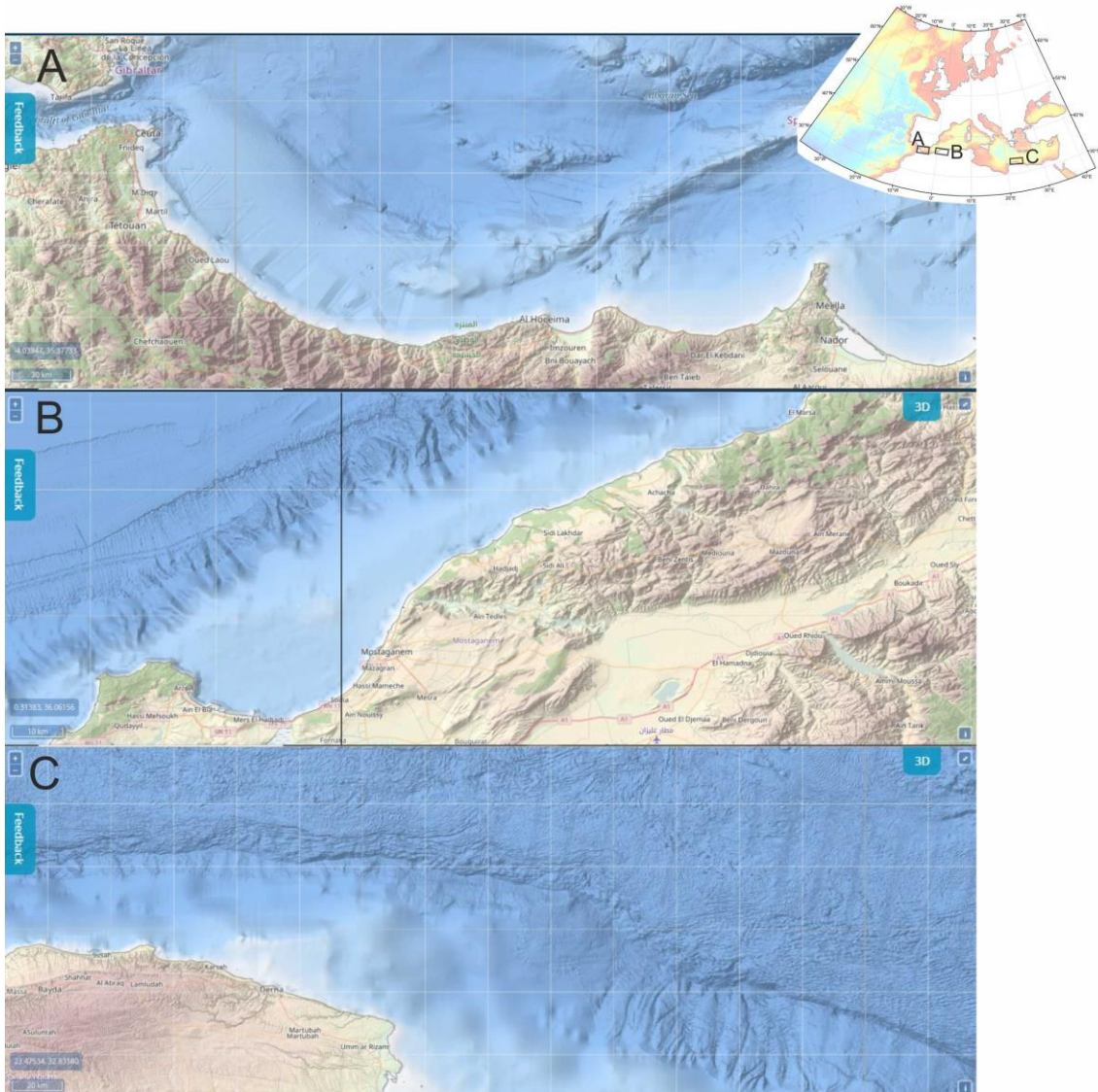


Fig. 3.7. Bathymetry models of the southeastern Mediterranean Sea. A. North of Morocco. B. North of Algeria. C. Northwest of Libya. D. Northeast of Libya. Source, EMODnet Bathymetry (<https://portal.emodnet-bathymetry.eu/>).

This information (per pixel) is not available on the web portal. Consequently, quantifiable targets to calculate knowledge gaps are not available. Nevertheless, areas with poor accuracy or lack of data were selected through a visual analysis (e.g. [Figs. 3.6c and 3.7](#)).

These areas were therefore classified as bathymetry knowledge gaps (**black dotted lines in Fig. 3.8**). However, most of these artefacts were not considered critical knowledge gaps in hydrate assessment, with the exception of those located north of Libya because of the low accuracy of the information and the presence of seabed fluid flow structures in the vicinity.

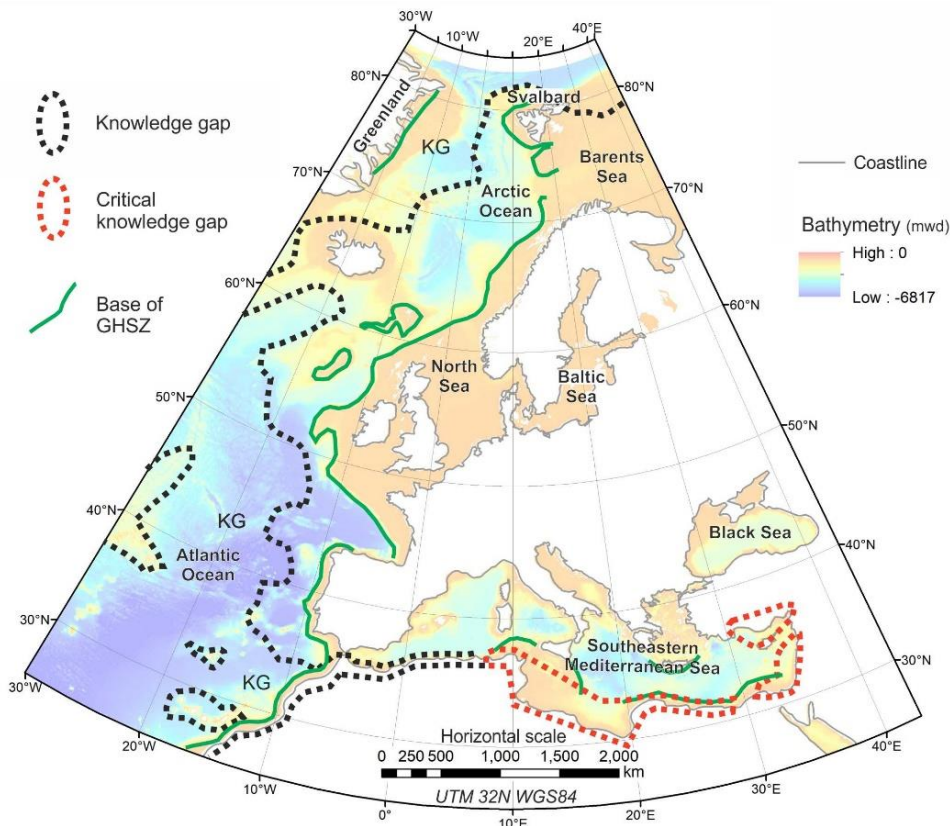


Fig. 3.8. Bathymetry knowledge gaps in the study area. KG, knowledge gap.

3.4. Sediment thickness

Sediment thickness establishes the geological framework in which hydrates are hosted and is therefore a constraint for hydrate thickness. Although the environmental conditions of temperature and pressure are optimal for reaching a particular thickness, this thickness will never be bigger than the sediment thickness. This dataset is therefore a useful tool as a geological constraint in many hydrate-related calculations.

In the study area, the Arctic Ocean and the Mediterranean and Black seas show areas without data that were catalogued as sediment thickness knowledge gaps (Fig. 3.9). In areas where hydrate evidence or BSRs have been detected, they were defined as critical.

We consider the lack of free public pan-European information on the porosity of the sedimentary units to be a knowledge gap. This is a critical point for higher porosity units (e.g. sands) that are capable of hosting more hydrate that represent an objective for CO₂ storage and a geohazard submarine feature.

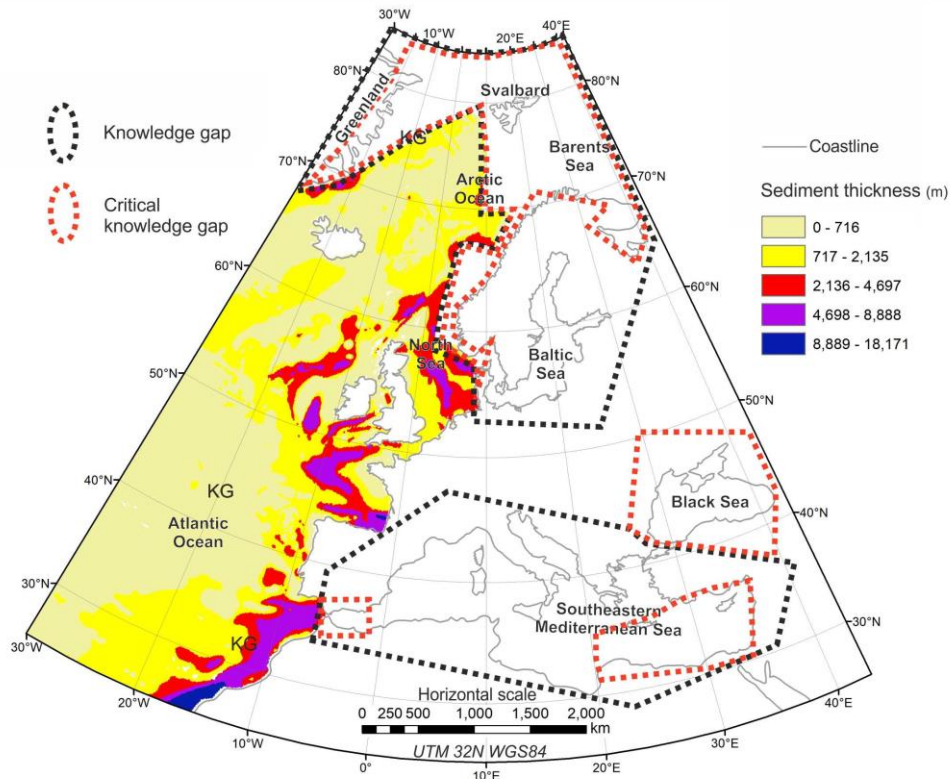


Fig. 3.9. Sediment thickness knowledge gaps in the study area.

3.5. Ocean production and sediment rate

The supply of methane for marine gas hydrate is commonly attributed to local conversion of organic material. In deep continental margin environments, sedimentation adds organic material to the region of hydrate stability. Conversion of the organic material to methane by bacteria promotes hydrate formation and depletes the supply of organic carbon (Kvenvolden, 1995; Sloan and Koh, 2008). The key parameters in this conversion are the sedimentation rate, the quantity and quality of the organic material, and a rate constant that characterizes the vigour of biological productivity (Davie and Buffet 2001).

Sediment rate

Free public pan-European data on the sedimentation rate were obtained from EMODnet Geology (Fig. 10; https://www.emodnet-geology.eu/map-viewer/?bmagic=y&baslay=baseMapEEA,baseMapGEUS&optlay=&extent=-2179400,-295790,7283560,5318790&layers=emodnet_sediment_accumulation_rates). Records of sedimentation rate show a non-uniform distribution with large knowledge gaps in the southern Mediterranean Sea, the deep Atlantic and Arctic

oceans and the Barents Sea (Fig. 11). The wide areas without data were classified as critical.

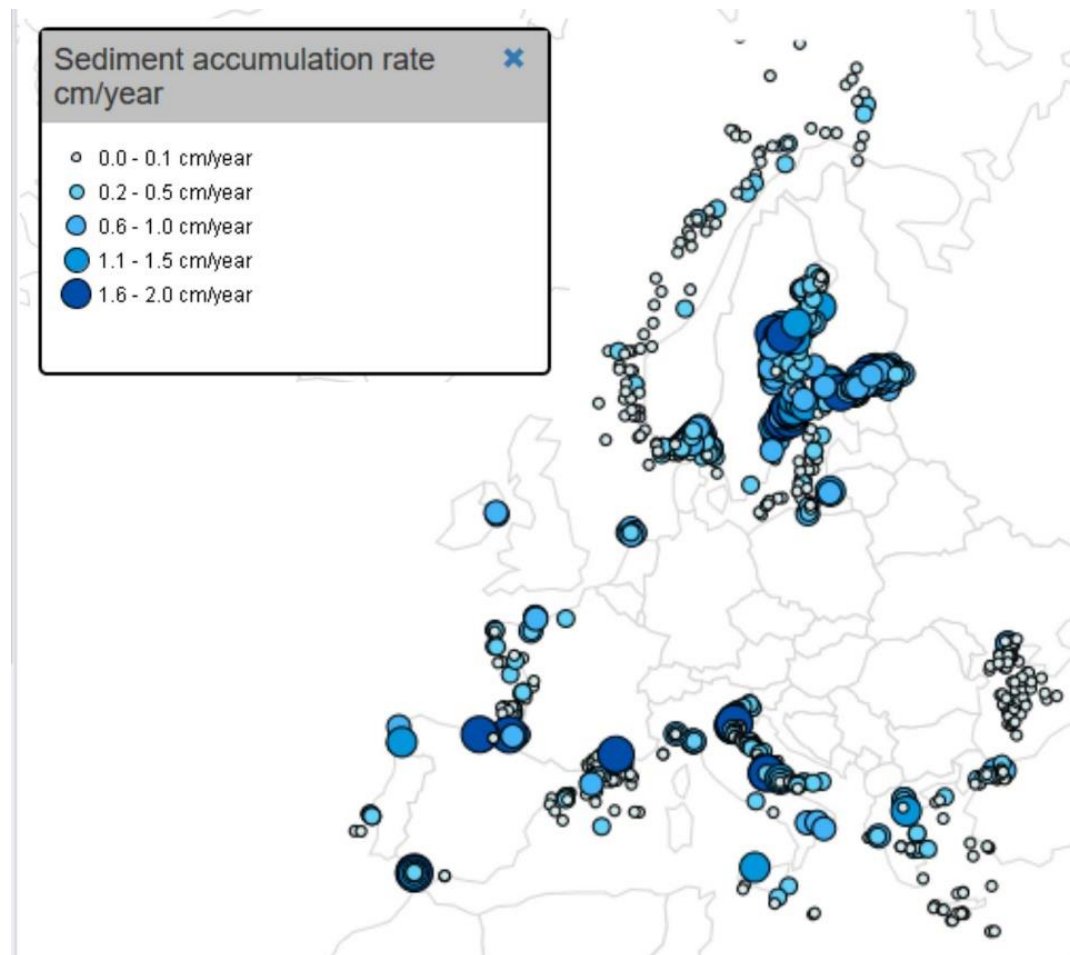


Fig. 10. Records of sedimentation rate along continental margins. Source, EMODnet Geology (<https://www.emodnet-geology.eu/>).

Nevertheless, it is difficult to understand the geographical meaning of this individual record without an information layer of sedimentary environments along the continental margins and adjacent areas. Proximal areas may have quite different sedimentation rates (e.g. flanks of a turbidite canyon and turbidite fans), and extensive areas may have similar sedimentation rates (e.g. abyssal plains or contourite drifts).

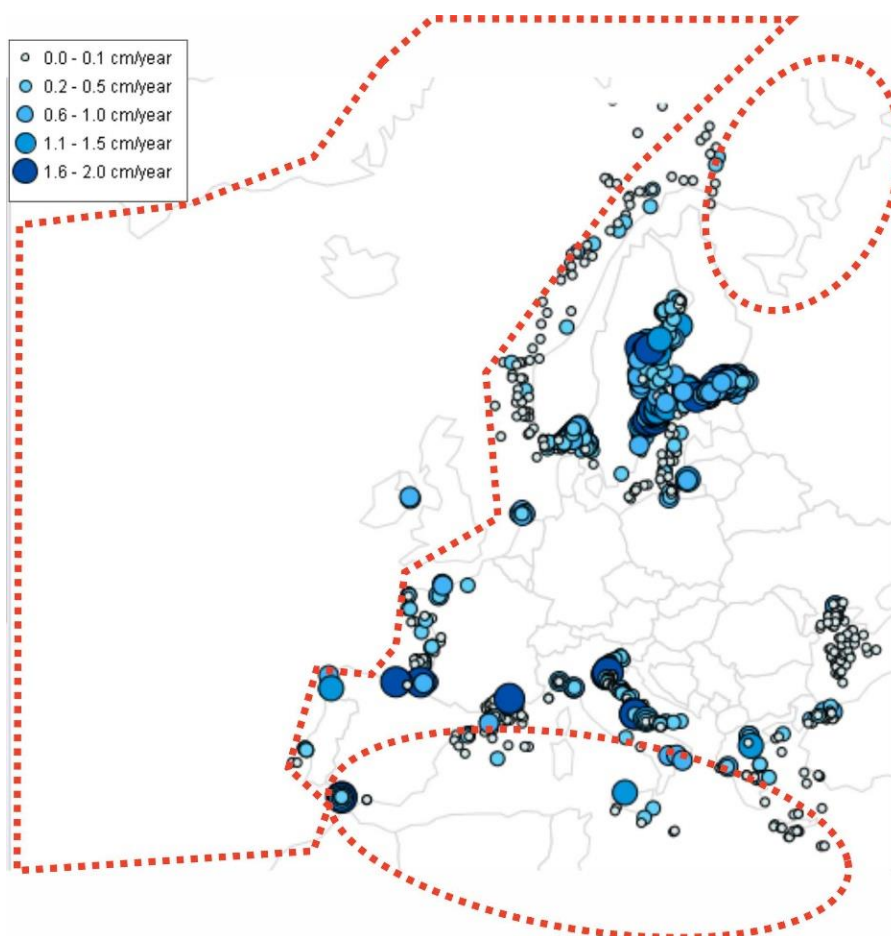


Fig. 11. Critical knowledge gaps in sedimentation rate. Source, EMODnet Geology (<https://www.emodnet-geology.eu/>).

Free public pan-European information is poor, non-continuous and incomplete. EMODnet Geology supplies valuable information, but this information should be re-thought in order to cover all the sedimentary environments of polygonal geographical features (Fig. 12). We suggest creating a single layer named “sedimentary environments”.

Ocean production

Free public global digital seafloor data on ocean production are not available. This is a general critical knowledge gap in the whole study area. Nevertheless, several models, such as analogical hardcopies (paper in PDF format), have been stored in the file system of the GIS related to seafloor organic carbon, CaCO₃ and MnO₂ (Archer et al., 2002; Daniels et al., 2018; Sulpis et al., 2018).

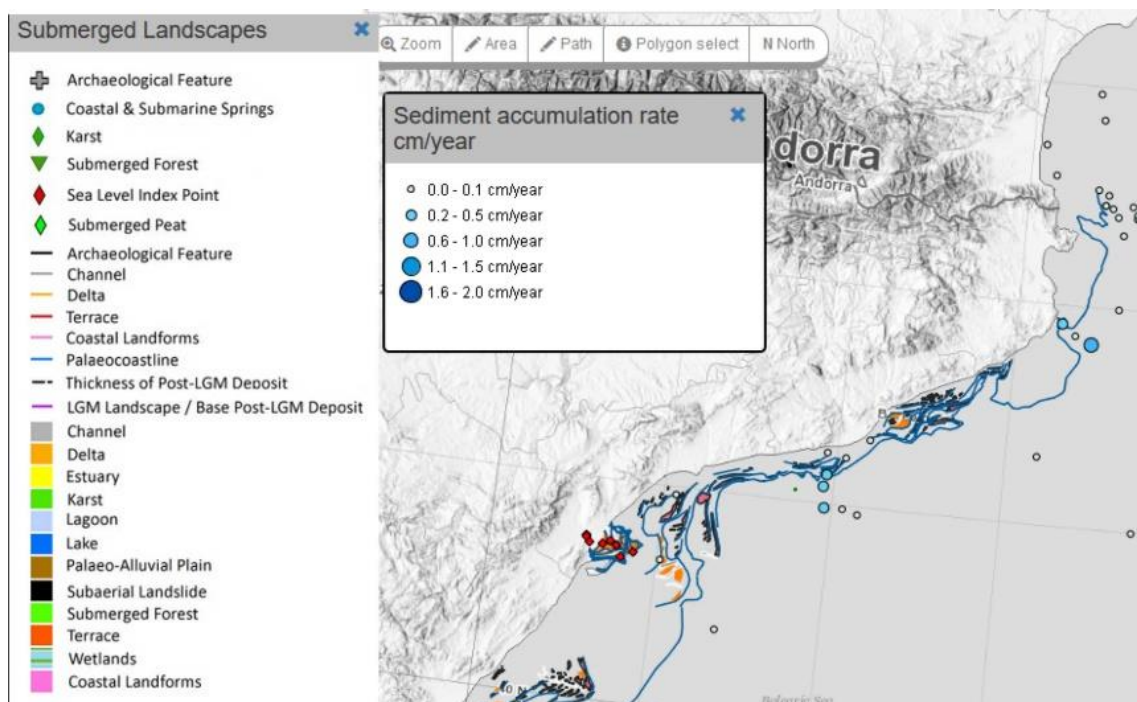


Fig. 12. Submerged landscapes and records of sedimentation rate along continental margins. Source, EMODnet Geology (<https://www.emodnet-geology.eu/>).

Owing to these critical knowledge gaps, the model of ocean primary productivity was added as an information layer. This model stores the photosynthetic rates ($\text{g C m}^{-2} \text{yr}^{-1}$) derived from satellite-based chlorophyll concentration (Behrenfeld and Falkowski, 1997). Spatial resolution, 5' (~7.5 km) and 10' (~15 km); temporal resolution, 8-day, monthly from 2002 to 2020; access, <http://sites.science.oregonstate.edu/ocean.productivity/standard.product.php> (cell size: 0.0833).

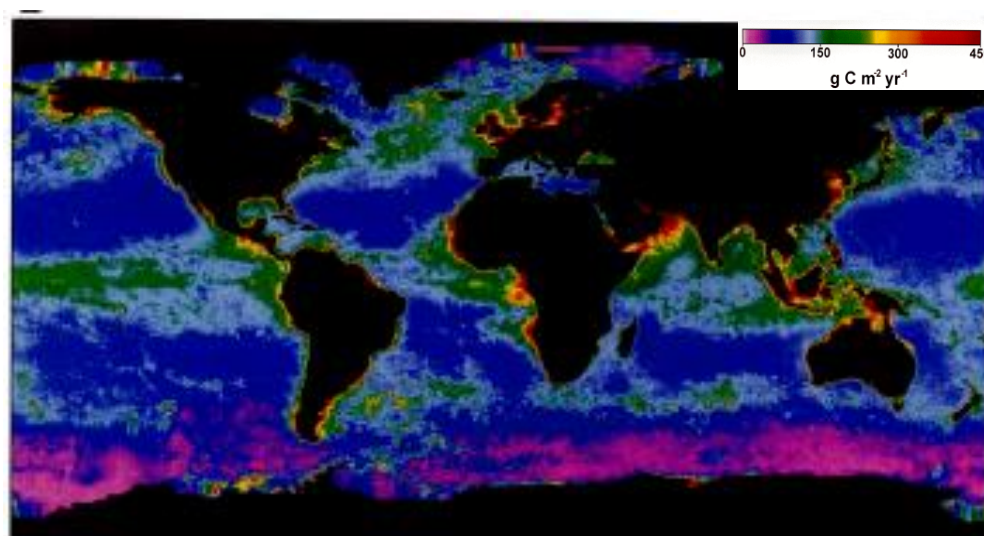


Fig. 13. Global estimates of annual phytoplankton primary production using the vertically generalized production model V(GPM).



4. AREAS OF INTEREST FOR FUTURE SCIENTIFIC PROJECTS

Hydrates are widespread in the ECMs from north to south (from the Arctic Ocean to the southern Iberian and north African margins) and from west to east (Greenland to the Black Sea). However, this project has revealed how hydrate-related data (geological, geophysical and oceanographic) are non-homogeneously covered in the whole extent of the ECMs. The study area therefore shows areas with a lack of data that have been catalogued as knowledge gaps. Locally, these knowledge gaps are located in areas with hydrate evidence and seepages or at the intersection between the seafloor and the theoretical base of the GHSZ. These areas have been catalogued as having critical knowledge gaps.

In our opinion, a fragile equilibrium of the hydrate stability conditions is indicated in areas located in the strip of intersection between the seafloor and the theoretical base of the GHSZ with (i) hydrate evidence and indicators, (ii) presence of seabed fluid flow structures such as mud volcanoes, pockmarks, collapses and gas flares in the sediment column, and (iii) authigenic carbonates. The rise of global temperatures in the last few decades and its future effect on the thermohaline circulation ([Clark et al., 2002](#); [Schmittner et al., 2005](#); [Vellinga and Wood, 2002](#)) make these areas especially vulnerable to dissociation processes ([Sloan, 2003](#)) and subsequently to seafloor instabilities such as collapses or landslides ([McConnell et al., 2012a](#); [Sloan, 2003](#)), or destruction of the extremophile ecosystems linked to these fluid leakage areas ([Cordes et al., 2009](#); [Foucher et al., 2009](#)).

In order to establish the seafloor areas of interest for future projects, two main factors were taken into account: critical knowledge gaps and hydrate evidence and indicators ([Fig. 4.1](#)). As described in Section 2, hydrate evidence and indicators in the study area are located in east Greenland, the Arctic Sea (Svalbard and the western Barents Sea), the northwest Norwegian margin, the northwest British Islands, the southern Iberian margin, the western Mediterranean Sea and the Black and Marmara seas. However, the seafloor shows areas with many critical knowledge gaps (e.g. seafloor temperature, geothermal gradient, bathymetry and sediment thickness).

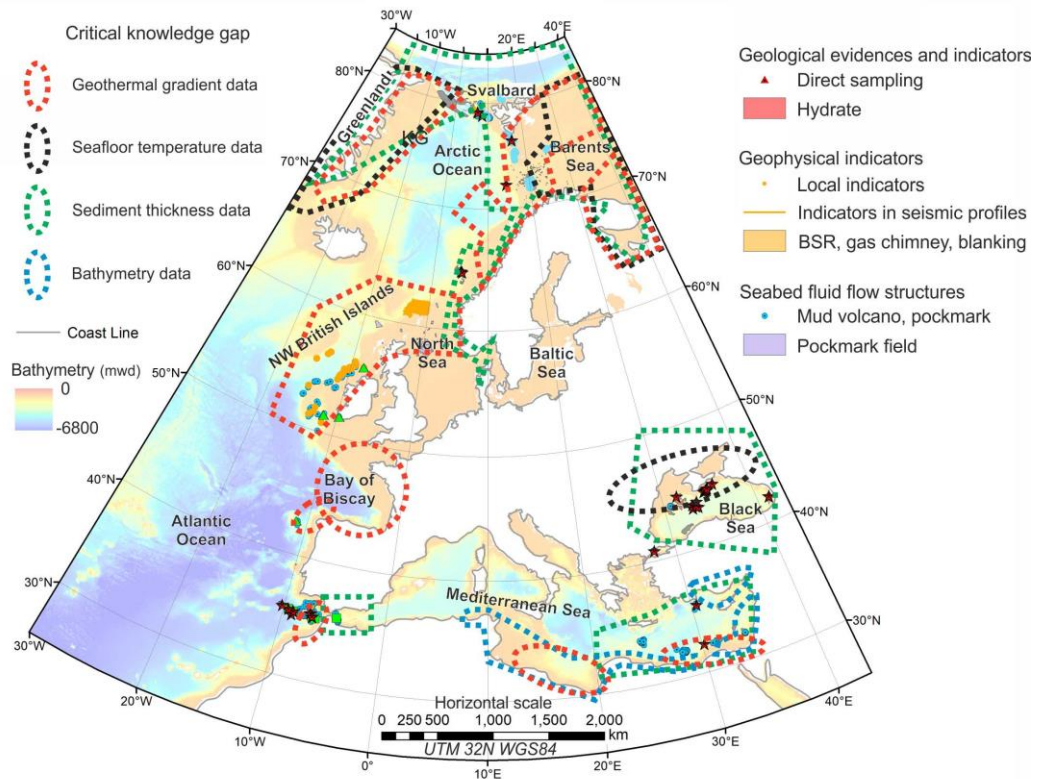


Fig. 4.1. Seafloor areas with knowledge gaps.

Taking into account these two factors (hydrate evidence and indicators and critical knowledge gaps), nine areas of interest for future scientific projects were defined (Fig. 4.2): east Greenland and Svalbard, the west Barents and White seas, the northwest Norwegian margin, the northwest British Islands, the Bay of Biscay and the northwest Iberian margin, the southern Iberian and northern Moroccan margins, the Tunisian and Libyan margins, the eastern Mediterranean, and the Black and Marmara seas.

East Greenland and Svalbard

This is an extensive area with several cases of hydrate evidence and indicators. It is also a remote and inaccessible place in winter and therefore suffers several critical knowledge gaps. Future research is needed in order to complete the geothermal gradient model in this geologically complex area and to determine the relationship between hydrates and some geophysical indicators such as BSR levels in east Greenland and west Svalbard.



The west Barents and White seas

This is the largest area with hydrate evidence and indicators in the Arctic Sea. However, further research is needed to develop detailed geothermal gradient and seafloor temperature models, especially in the White Sea, where several critical knowledge gaps have been evidenced in this project.

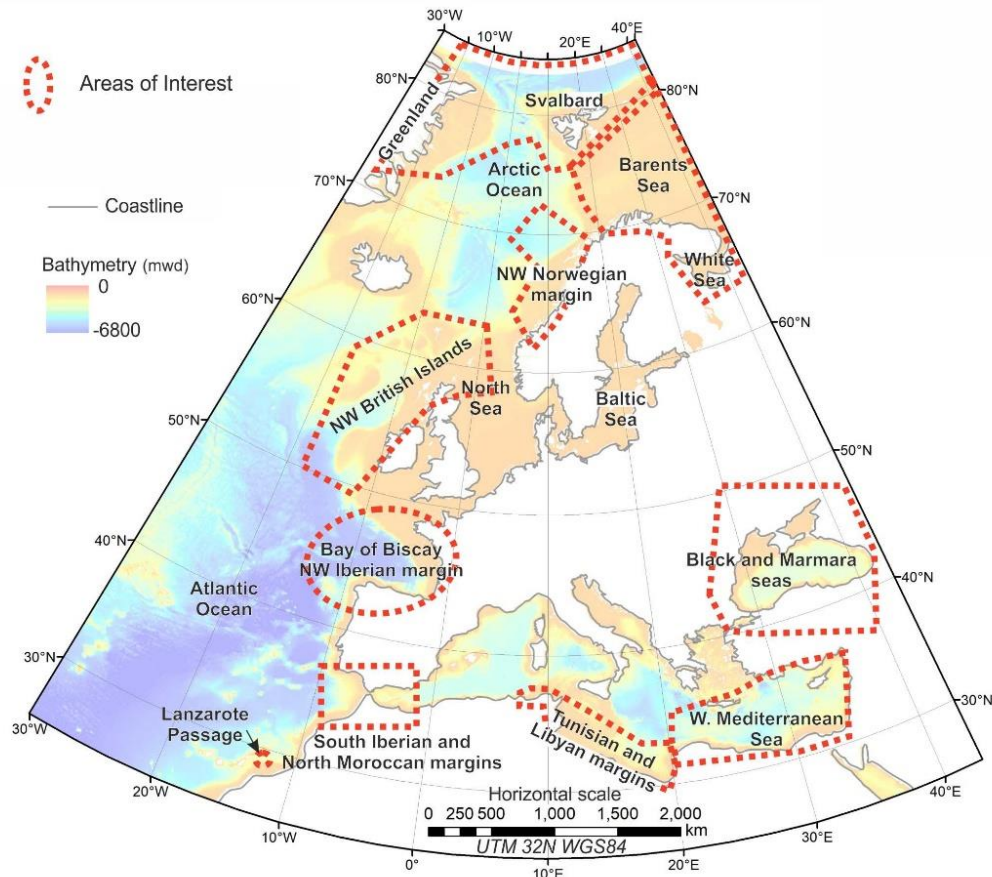


Fig. 4.2. Areas of interest for future scientific projects.

The northwest Norwegian margin

This area is located in the vicinity of the headwall scarp of the Storegga mega-landslide. Here, BSR levels, pockmarks and landslides are observed and constitute a natural laboratory for future projects to investigate the past and future role of gas hydrates in constructive and destructive geological processes on the continental margins.



The northwest British Islands

Although no hydrates have been detected in the northwest British Islands, several hydrate indicators, both chemical and seismic, were extensively reported in this project. In addition, this area is located inside the marine methane GHSZ (Roy et al., 2018). Thus, we consider this area as a subject for future research in order to understand the relationship between hydrates and the indicators found and to assess their role in safe storage of CO₂ and submarine geohazards.

The Bay of Biscay and the northwest Iberian margin

As in the northwest British Islands, no hydrates have been found. Furthermore, except on the Galicia Bank (northwest Iberian margin), no hydrate indicators have been found in the whole extent of the Bay of Biscay. However, the continental slope and deeper areas of the Bay of Biscay and the northwest Iberian margin are located inside the marine methane and CO₂ GHSZ (Burnol, 2018). We therefore consider this area of interest for further scientific projects in order to create a detailed geothermal gradient and seafloor temperature models, as well as to investigate the role of hydrates (marine methane and CO₂) in safe CO₂ storage and submarine geohazards.

The southern Iberian and northwest Moroccan margins

The southern Iberian and northwest Moroccan margins are the areas of the Atlantic Ocean where the most direct evidence of hydrates (samples of hydrates) has been reported. Furthermore, in the Gulf of Cádiz in particular, hydrates are present in focused fluid flow structures (mud volcanoes and a warm water mass, the Mediterranean Outflow Waters, affect the seafloor with the subsequent effect on the thickness of the GHSZ) (León et al., 2009). We therefore consider this to be an area of interest for further scientific projects in order to investigate (i) the migration of the gas system from the focused mud volcano system to the sedimentary column, (ii) the role of the possible gas hydrate system inside contourite depositional systems (Hernández-Molina et al., 2011) and (iii) the effect of the warm Mediterranean Outflow Waters on the gas hydrate system.

The area named the Lanzarote Passage (Vázquez et al., 2015) was selected as an area of interest because of its location inside the GHSZ, the lack of information and the presence of hydrocarbon seabed fluid flow structures and fragile related ecosystems.



The Tunisian and Libyan margins

We consider this an area of interest because of the critical knowledge gaps detected and the proximity of hydrocarbon evidence both onshore and offshore.

The eastern Mediterranean Sea and the Marmara Sea

In the eastern Mediterranean Sea, direct evidence of hydrates has been reported in focused fluid flow structures. Seismic and chemical indicators have also been reported, in addition to pockmark fields. Multiple critical knowledge gaps were found in this project (e.g. geothermal gradient, seafloor temperature and sediment thickness and rate). It has therefore been proposed as an area of interest for future scientific projects in order to understand the role of hydrates in seabed fluid flow and sedimentary-structural systems.

The Black Sea

In the Black Sea, direct evidence and geophysical indicators of hydrates (e.g. BSRs) have been reported. In addition, 91% of its seafloor is inside the GHSZ ([Vassilev and Dimitrov, 2002](#)). Physical sediment parameters, heat flow measurements, geochemical data and sediment dating are required to calibrate the remote sensing techniques and to allow the available models to be extended along the margin ([Minshull et al., 2020](#)). For the above reasons, the Black Sea is an interesting target to be a natural laboratory for a European hydrate field study.



5. POTENTIAL SAFE GEOLOGICAL STORAGE OF CO₂ AS MIXED GAS HYDRATES

The public acceptance will be key to enable the large deployment of the carbon capture and storage (CCS) technology. Offshore storage would be easier to be implemented with regards to public acceptance but will be more expensive than onshore storage (Alazard-Toux et al., 2015). Storage costs are site dependent and vary from 1 to 20 €/ton according to whether storage is operated onshore (cost in the low range) or offshore (cost in the high range). A first economic evaluation in the United States case concluded that offshore and deep offshore (>3,000 m water depth) storage including transport and injection are likely to be two and three times as expensive as onshore storage, respectively (Eccles and Pratson, 2013). However, a comprehensive comparative study should consider all the associated costs, such as the potential conflicts of use (e.g. potential interferences with potential geothermal exploitations in the same geological formations), the applicable regulations related to social acceptability and the monitoring costs from the end of the injection through the entire storage life. The deployment perspectives between 2020 and 2050 of the three different CO₂ storage technologies are qualitatively estimated in Table 5.1.

	2020	2030	2040	2050
Onshore geological storage	3	4	4	4
Offshore geological storage	3	4	5	5
Deep offshore geological storage	1	2	3	4-5

The maturity level is the TRL, reduced to 5 levels with market deployment enclosed in the higher TRL classes; maturity level scaling: 0 = none; 1 = fundamental research; 2 = R&D; 3 = demonstrator; 4 = low deployment; 5 = large deployment

Table 5.1. Maturity level and perspectives of CO₂ storage technologies (modified from Alazard-Toux et al., 2015)

Deep saline aquifers are the most important onshore or offshore potential geological reservoirs for CO₂ storage under supercritical conditions (i.e. a pressure higher than 7.4 MPa and a temperature higher than 31°C). In the period up to and including 2021, there is more in Europe offshore storage pilots (e.g., Sleipner, North Sea since 1996, Snøhvit, Barents Sea since 2009) than onshore pilots (e.g. French Lacq-Rousse pilot during the period 2006–2013). Because the density of supercritical CO₂ is lower than that of pore brine water, the storage efficiency depends on the sealing capacity of the overlying tight formations (the so-called “cap rock”) with respect to a non-aqueous buoyant fluid (CO₂ and associated impurities). In the hypothetical case of a CO₂ leak from the target reservoir, some trapping mechanisms in the overburden may play a role including



the dissolution into interstitial brine, the residual trapping and, in some specific conditions (e.g. Snøhvit, Barents Sea), the formation of CO₂-containing gas hydrates (Burnol, 2018) (see also D2.6 GARAH report “Alternative uses and risks”).

Another storage option (the so-called “deep offshore” option) is the trapping of CO₂ in deep-sea sediments at lower temperature (2–15°C) and higher pressure (40–60 MPa) than the standard conditions in the onshore and offshore storage options. The “deep offshore” storage option and the method for inferring the main phase (either liquid or solid as mixed gas hydrates) in which the CO₂ is stored is described in Section 5.1. The storage capacity in the French and Spanish Exclusive Economic Zones (EEZs) in the area of the Biscay Bay and Galicia Plateau (Burnol, 2018) is estimated in Section 5.2.

5.1. The “deep offshore” CO₂ storage as mixed gas hydrates

In the “deep offshore” storage option, the CO₂-rich fluid (CO₂ with the associated impurities) may be liquid and denser than seawater. In that case, the injected liquid CO₂ may be gravitationally trapped in the deep-sea sediments, either in the liquid state or in the solid state as gas hydrates. This deep offshore option is currently much less investigated in the literature, even though it may offer advantages in terms of capacity, safety and long-term containment of CO₂ (e.g. Burnol et al., 2015; Koide et al., 1995; Rochelle et al., 2009).

The safety of a “deep offshore” CO₂ will depend on the density of the injected CO₂ (included the impurities). Assuming 3.6 mol% of nitrogen in CO₂ stream (Table 5.2), the liquid density of this CO₂-rich fluid is higher than seawater below about 4,000 m water depth (Figure 5.2). The bottom water temperature along the continental rise and the abyssal plain is almost constant (e.g. the mean value in the French EEZ is around 2.5°C). The seawater density is calculated by the 1980 International Equation of State (EOS-80) assuming that the salinity is almost constant along the vertical profile (e.g. S = 34.92 in the French EEZ).

Mole fraction (%)	CO ₂ -100 (Pure CO ₂)	CO ₂ -96
CO ₂	100	96.4
N ₂	0	3.6

Total volume for all non-condensable gases together (N₂, Ar, H₂, CH₄, CO, O₂) is recommended to be less than 4% (volume fraction) in CO₂ for CCS (de Visser et al., 2008)

Table 5.2. Pure CO₂ (CO₂-100) and CO₂-96 stream compositions

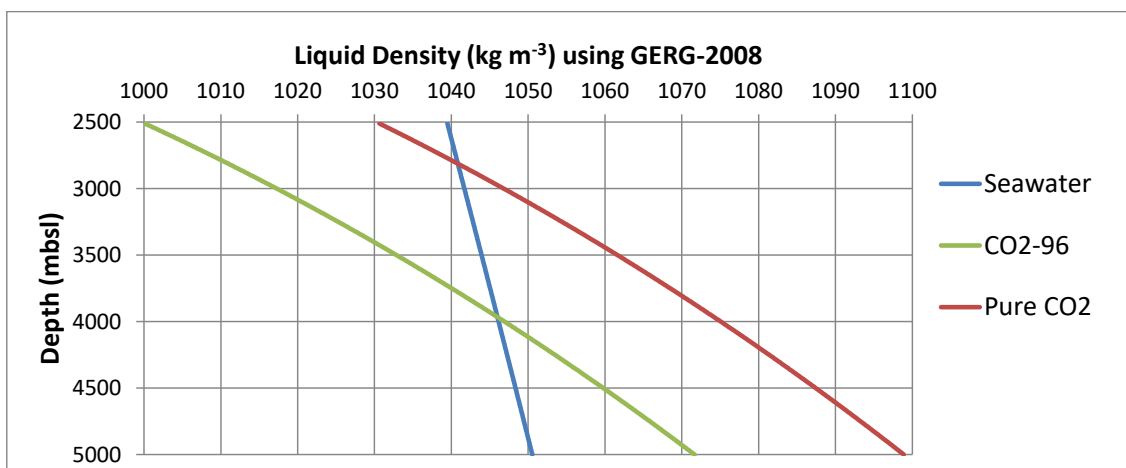


Fig. 5.1. Variation with depth of the liquid density of pure CO₂ and CO₂-96 calculated by GERG-2008 (Kunz and Wagner, 2012) and comparison with the seawater density calculated by the 1980 International Equation of State (EOS-80) assuming a mean bottom water temperature of 2.5 °C and a mean salinity of S = 34.92 in the French EEZ

In that case, below about 4,000 m water depth, the injected CO₂ may be therefore gravitationally trapped in the deep-sea sediments, either in the liquid state or in the solid state as gas hydrate. The ice-like hydrate phase can even clog pore space and cement grains, therefore reducing the permeability and forming a mechanically strong “self-sealing” cap in the overburden (House et al., 2006; Tohidi et al., 2010). Consequently, there is no need in that storage option of an overlying “cap rock”, but only the need of sufficient high permeable sediments in deep-sea regions (Levine et al., 2007).

The negative buoyancy zone (NBZ) is determined by calculating the density difference between the seawater and the CO₂-rich mixture (CO₂-N with N = 96, 100). The GHSZ is determined by calculating the difference between the gas hydrate equilibrium pressure (depending on the sediment temperature T) calculated by the CSMGem code Version 1.10 (January 1, 2007) (Sloan and Koh, 2007) and the pore water pressure (depending on the depth z and the latitude) given by the Saunders’s formula (Saunders, 1981). The code “GASCO2” has been used to calculate the thickness of NBZ and GHSZ for each case using GERG-2008 and CSMGem, respectively (Burnol et al., 2015). The state of the stored CO₂ (liquid or solid as mixed gas hydrates) depends mainly on three parameters: the heat flow, the seafloor depth and the CO₂ quality (Figure 5.2). If the thickness of NBZ is larger than the thickness of the GHSZ, the injected CO₂(l) is expected to percolate downwards to the bottom of the NBZ and will accumulate on either side of the neutral buoyancy level, with the depth of CO₂ above the level matching the depth below it (Levine et al., 2007). As shown in Figure 5.2, it is indeed always the case below 4,000 m for pure CO₂ but it will depend on the seafloor depth for CO₂ with 4% vol. of impurities (CO₂-96).

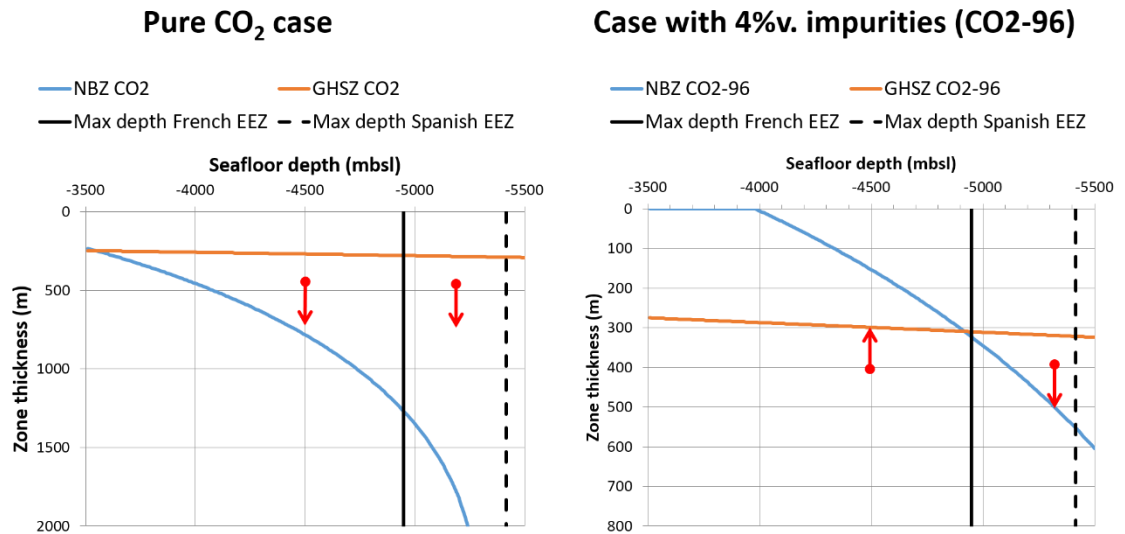


Fig. 5.2. Influence of the seafloor depth (below 3,500 m water depth) on the thickness of NBZ and GHSZ with pure CO₂ or CO₂-96 assuming a bottom water temperature of 2.5°C and a local heat flow of 46.5 mW/m². The red arrow indicates the vertical direction of the buoyancy-driven migration after injection of a CO₂-rich liquid at about 450 m. The solid and dotted black line is the maximum depth in French and Spanish EEZ, respectively.

5.2. Potential safe CO₂ deep offshore storage capacity in the French and Spanish EEZs

In [Figure 5.3](#), the high resolution of the EMODnet bathymetry, with a grid-size of 1/8×1/8 minutes (circa 230 m) has been used to define a potential interesting zone for a safe deep offshore CO₂ storage by considering a set of three safety criteria ([Burnol, 2018](#)):

- 1) a water column depth higher than 4,000 m to ensure that the density of the injected fluid is higher than the seawater density ([Figure 5.1](#))
- 2) a seafloor dip angle lower than 4° to avoid the risk of slumps coming from the continental slope
- 3) a sediment thickness of at less 800 m.

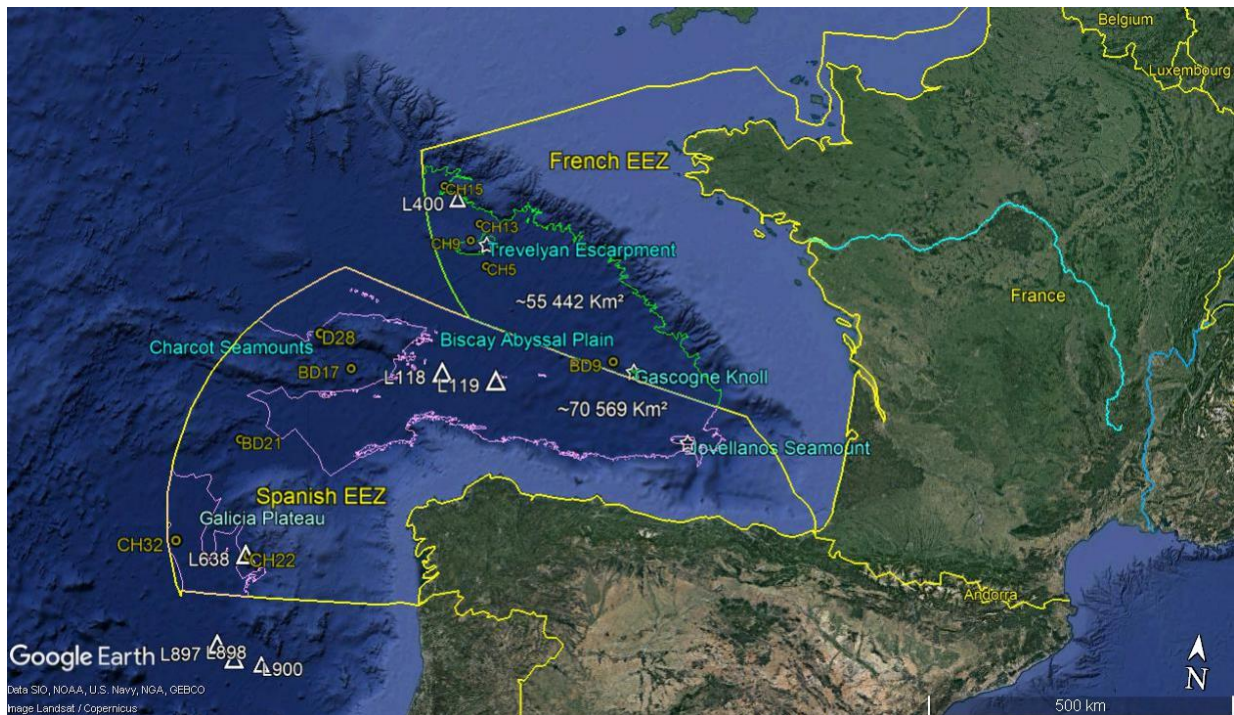


Figure 5.3. Map of the area of the Bay of Biscay and Galicia Plateau showing locations of both CO₂ storage zones in the French EEZ (in green) and in the Spanish EEZ (in pink) after applying the three safety criteria described in the text. Also shown are some boreholes (e.g. L400) and other data (e.g. BD9) physiographic features of interest in the studied area: (1) Trevelyan Escarpment, (2) Gascogne Knoll, (3) Jovellanos Seamount, (4) Charcot Seamounts and (5) Galicia Plateau.

The Generic Mapping Tool (GMT) (Wessel and Smith, 1998) has been used to apply these three criteria and to calculate the storage surfaces in both zones, i.e. 55,443 km² in the French EEZ and 107,289 km² in the Spanish EEZ (Table 5.3). By definition, the theoretical storage volume is the total physical porous volume that may host the CO₂-rich phase (gas hydrate or liquid). It assumes that the entire volume is accessible and utilized to its full capacity to store in the pore space. It represents therefore a maximum upper limit to a storage volume estimate (and therefore unrealistic to calculate the storage capacity). GMT has been also used to calculate the theoretical storage volumes in both zones: the theoretical storage volume is the product of the three parameters (surface, thickness and porosity).

The French EEZ storage volume estimate of 3,422 km³ is of the same order of magnitude as the total storage volume in the Spanish EEZ estimate of 3,700 km³ (Table 5.3). There is, however, a big difference resulting from the seafloor depth: in the French case, almost all the stored volume is occupied by gas hydrates, whereas in the Spanish case, about the half (1,728 km³) is occupied by CO₂ in hydrate phase and the other half (1,972 km³) by liquid CO₂ (Table 5.3).



		Surface ^a (km ²)	Mean thickness ^b (m)	Mean porosity	Theoretical storage volume (km ³)
French EEZ (CO ₂ -100)	Liquid	55,443	1213	0.3	20,173
French EEZ (CO ₂ -96)	Gas hydrate	55,442	115	0.53	3,422
Spanish EEZ (CO ₂ -96)	Gas hydrate	70,569	52	0.45	1,728
	Liquid	36,720	153	0.39	1,972

^A Surface of CO₂-96 storage as gas hydrates is the subdomain where NBZ is included in GHSZ, and surface of CO₂-96 storage as a liquid is the subdomain where GHSZ is included in NBZ.

^B Vertical thickness of the CO₂-96 storage volume, either in the liquid state or as gas hydrate: as a liquid, the thickness is twice the depth difference between the neutral buoyancy level and the gas hydrate formation level as gas hydrate, the thickness is the difference between the hydrate formation level and the neutral buoyancy level.

Table 5.3. CO₂ storage capacity in the French EEZ and in the Spanish EEZ

5.1. Conclusions and perspectives

There is still a need for a precise description of the physical and chemical behavior of the injected fluid (liquid mixture of CO₂ and different impurities like H₂S) in the high-pressure range (between 40 and 60 MPa) with respect to the geological matrix. In particular, the variable fraction of clay in the deep-sea sediments on the gas hydrates formation may play an important role for the injectivity and the effective storage capacity. Large uncertainties remain with regard to the effective storage capacity due to the lack of knowledge of the influence of the sediment composition on the mixed gas hydrates formation kinetics and on the saturation level in the deep-offshore conditions. Molecular dynamics simulation may offer insights into atomic level mechanisms in high pressure conditions (40–60 MPa) that are not easily observable from an experimental point of view, for instance to study the influence of different types of clay surfaces on CO₂ hydrates formation kinetics. Thus, more experimental and modeling works still need to be done for a better understanding of the potential roles of gas hydrates for CO₂ geological storage.



6. HYDRATE-RELATED GEOHAZARDS

Marine gas hydrates are ice-like crystalline solids containing a mixture of hydrocarbon gases with low molecular weight, such as methane (the most common), ethane and propane, bound with water molecules within cage-like lattices (Paull et al., 2015). Marine sediments can host these gas hydrate lattices under a specific range of high pressures and relatively low temperatures and abundant gas (Sloan, 1998; You et al., 2019). Gas hydrates are commonly found in the shallow sediment (<~1,000 m below the seafloor) along continental margins at water depths greater than ~350 to 600 m, and within and beneath permafrost and glaciers where there is sufficient methane available (Boswell et al., 2014; Kvenvolden, 1988; Sloan, 1998). Bacterial methanogenesis and thermogenesis are the main source of CH₄ in continental margin sediment (Dickens, 2001).

Massive hydrate dissociations triggered in natural scenarios such as drops in sea level and warming of bottom water can generate seafloor instabilities such as landslides, pockmarks, collapses and seafloor explosions (Sloan, 1998). However, gas hydrate dissociation processes can also be triggered by human activity, including wellheads and pipelines (McConnell et al., 2012b). Thus, future climate scenarios and global warming will place the now-stable gas hydrate deposits in marine sediments and permafrost as a serious future geohazard (Maslin et al., 2010).

One of the main knowledge gaps of hydrate-related information is the lack of a pan-European assessment of the hydrate-related risk. In this section, a pan-European assessment of hydrate-related risk was carried out in order to assess the impacts of possible destabilization of hydrates on the seafloor and potential links with geohazards. The risk analysis was performed to assess the susceptibility of the seafloor to being affected by hydrate dissociation processes, both natural and human-induced.

6.1. Susceptibility map assessment of seafloor areas affected by hydrate dissociation

The susceptibility map assessment of seafloor areas affected by hydrate dissociation shown in this subsection is based on the data stored in the GIS database of the GARAH project. Several factors and variables were taken into account in this assessment. The following is a description of each factor and variable analysed in this work.



Hydrate evidence. Hydrate evidence is the ground truth of where hydrate exists. This layer establishes seafloor areas with a moderate to high likelihood of occurrence of dissociation processes on or below the seafloor. The magnitude of the processes will depend on the quantity of hydrate in the sedimentary column and its type inside the sediment (massive, in layers, disseminated, etc.).

Seismic indicators. Seismic indicators show seafloor areas where hydrate could exist. Hydrates have not been recovered but there is a moderate to high likelihood of their occurrence. In areas where hydrates have been recovered (hydrate evidence), seismic indicators allow the occurrence of hydrates to be inferred.

Seabed fluid flow structures. Seafloor geological structures related to hydrocarbon fluid migration, such as pockmarks, gas flares, mud volcanoes and hydrocarbon-derived authigenic carbonates, are directly linked to deep hydrocarbon reservoirs. The occurrence of these structures reveals a free fluid leakage from the sedimentary structure to the water column or hydrate dissociation processes. Depending on its position (inside or outside the GHSZ), this layer of information will establish a wide spectrum of susceptibility to seafloor hydrate dissociation. It will therefore range from low or null in areas outside the GHSZ to high in areas inside the GHSZ.

Thickness of the GHSZ. The thickness of the GHSZ establishes the theoretical seafloor area where the occurrence of hydrates is physically possible under optimal gas saturation and salinity conditions. Seafloor areas inside the GHSZ will be considered potential areas to be affected by dissociation processes. Furthermore, the intersection between the base of the GHSZ and the seafloor is a potential strip of high likelihood of occurrence of fluid leakage and dissociation processes. The thickness of the GHSZ was calculated by applying the model of [León et al. \(2009\)](#). Three oceanographic variables were taken into account: seafloor temperature, geothermal gradient and bathymetry.

Seafloor temperature. The thickness of the GHSZ depends greatly on seafloor temperature changes ([Dickens, 2001](#); [Kvenvolden, 1988](#); [León et al., 2009](#); [Sloan, 1998](#)). A reliable digital model of the bottom seawater temperatures was developed with the data stored in the seafloor temperature layer in the GARAH GIS hydrate database (deliverable D3.2 of GARAH project). The digital model of the bottom seawater temperatures was conceived as a mosaic of seafloor areas under the influence of different European water masses ([Núñez-Varela 2020](#)).



Geothermal gradient. Under suitable temperature, salinity and pressure conditions (inside the GHSZ), methane hydrates can only crystallize from natural gases when gas concentrations exceed the methane solubility in the sediment porewater (Sloan, 1998; Davie and Buffett, 2001). The base of the GHSZ (Fig. 6.1) is controlled by the increase in temperature due to the geothermal gradient (Claypool and Kaplan, 1974; Kvenvolden, 1988, 1995). A numerical surface representative of the geothermal gradient of at least the first 200 m of the sub-seafloor was developed (Núñez-Varela 2020) in order to evaluate the thickness of the GHSZ from the information on the geothermal gradient layer stored in the GARAH GIS hydrate database (deliverable D3.2).

Bathymetry. Bathymetry controls the pore pressure conditions inside the sediments (León et al., 2009; Piñero et al., 2013; Wallmann et al., 2012). The bathymetry model was taken from EMODnet Bathymetry (“EMODnet Bathymetry,” n.d.).

Salinity. Salinity is an inhibitor of gas hydrate nucleation. Gas hydrates stability decreases with increasing salinity. In this way, salt domes prevent gas hydrate formation (Burnol, 2018; Sloan and Koh, 2007).

Control factors and constraints

Several factors were taken into account in order to carry out the susceptibility assessment. A group of factors was defined by the geological and geophysical evidence and indicators related to the presence of hydrates below the seafloor. Each piece of evidence and indicator was weighted depending on the confidence/certainty of finding hydrates at the site. The maximum weighting (or confidence) was given to the recovered samples of gas hydrates or hydrate dissociation evidence such as degassing or liquation structures observed in gravity cores. Seismic indicators of the presence of gas hydrates or hydrocarbon seabed fluid flow such as BSRs, acoustic blanking, amplitude anomalies or the presence of geological structures of seabed fluid flow in the vicinity of the GHSZ were weighted with a lower value (Table 6.1).



Evidence and Indicator	Description	weight
Gas hydrate samples	Crystals or aggregates of gas hydrates observed in gravity cores.	1
Degassing and/or liquation structures	Bubbles and/or vacuoles (porosity) in sediment liquefactions observed in gravity core samples.	1
Pore water anomalies	Chemical and isotopic pore water anomalies that are caused by hydrate dissociation (e.g. downward chlorinity decrease combined with $\delta^{18}O$ increase).	0.9
BSRs	Only bottom-simulating reflectors generated by the impedance contrast between the gas-hydrated sediment above and a free gas layer below. Opal BSRs are excluded.	0.9
High resistivity	Anomalous high electrical resistivity in logs due to the presence of massive hydrates.	0.9
Velocity anomalies	Anomalous seismic propagation velocity in the sediment due to the presence of both gas hydrates and free gas.	0.8
Blanking acoustic	Zones devoid of reflections in seismic profiles because of the presence of free gas in the sediment.	0.8
Dim zones	Local low-amplitude seismic attribute anomalies that may indicate the presence of hydrocarbons.	0.8
Bright spots	Seismic amplitude or high-amplitude anomalies that may indicate the presence of hydrocarbons.	
Gas chimneys	Areas of poor data quality or push-downs caused by subsurface leakage of gas from a poorly sealed hydrocarbon accumulation.	0.8
Seabed features	Geomorphological features related to seabed fluid flow.	0.8
Gas seepages: pockmarks, mud volcanoes	Steady or episodic, slow or rapid, visible or invisible flow of gaseous hydrocarbons from subsurface sources to the Earth's surface. Pockmarks are craters in the seabed caused by fluids erupting and streaming through the sediments. Mud volcanoes are positive cone-shaped reliefs created by the extrusion of mud, water and gases, mainly hydrocarbon fluids.	0.8
Mud diapirs	Positive, cone-shaped reliefs created by intrusion inside the sediment column of mud, water and gases, mainly hydrocarbon fluids.	0.8
MDAC	Methane-derived authigenic carbonate (MDAC) formed as a consequence of the anaerobic oxidation of methane by consortia of microbes.	0.8
Gas flares	Acoustic artefacts in the water column caused by gas bubbles.	0.8

Table 6.1. Weightings given to each hydrate-related evidence or indicator for the development of the density map of evidence/indicators.

Finally, the theoretical GHSZ for a standard composition of biogenic gas defined by [Núñez-Varela \(2020\)](#) was taken into account as another control factor and constraint feature. The physical constraint is defined by the location of the seafloor with respect to the GHSZ. Seafloor areas outside the theoretical GHSZ were excluded as likely to be affected by hydrate dissociation processes. On the



other hand, any location inside the GHSZ was selected as theoretically likely to suffer dissociation processes. Nevertheless, the base of the GHSZ was classified as a critical area for these dissociation processes (Fig. 6.1) with a weighting of 1, whereas the rest of the GHSZ had a weighting of 0.25.

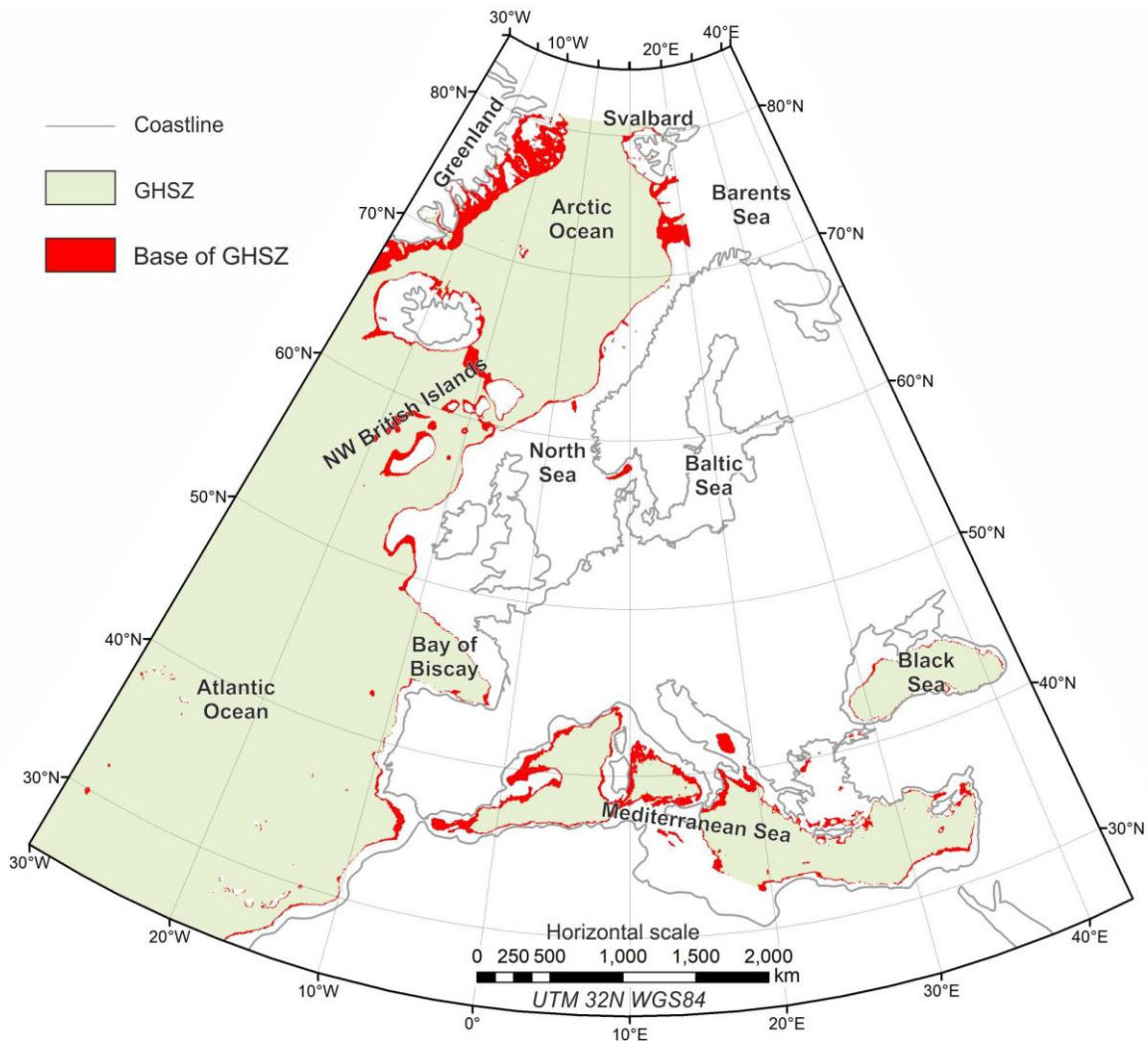


Fig. 6.1. Seafloor areas inside the GHSZ (Modified from Núñez-Varela, 2020) weighted for the susceptibility assessment for the occurrence of hydrate dissociation processes.

Susceptibility assessment

The proposed methodology analyses the geological hazard by means of the susceptibility assessment. The term “susceptibility” is employed here to define the likelihood of occurrence of hydrate dissociation, collapses, crater-like depressions or submarine landslides on the seafloor. Susceptibility assessment is applied as the first step in a pan-European risk assessment, owing in particular to (i) the regional scope of the assessment (the ECMs and adjacent areas) and



(ii) the current state of European gas hydrate–related information characterized by areas intensively studied with a high density of high-quality data and wide areas of critical knowledge gaps with no data.

The baseline scenario (the initial hypothesis) is that gas hydrate occurrence is only possible in seafloor areas where pressure (bathymetry) and seafloor temperature conditions are inside the theoretical GHSZ. Inside the GHSZ, the occurrence of gas hydrate is directly related to the presence of evidence (direct samples of hydrates) or indicators of it (e.g. pore water and velocity anomalies, BSRs and gas chimneys), as well as the occurrence of hydrocarbon fluid flow structures. Finally, the likelihood of the seafloor being affected by gas hydrate dissociation processes will be great at the base of the GHSZ and in the vicinity of gas hydrate evidence and indicators.

In order to prove this initial hypothesis, a susceptibility assessment was carried out through map algebra in a GIS environment from a density map of evidence and indicators and the pan-European map of the GHSZ on the seafloor.

Density map of evidence and indicators

The first step for the development of the density map was to create a lattice of evidence and indicators at a resolution of the work scale (5 km x 5 km), which will be the final resolution of the susceptibility assessment map. In this lattice, each geographical feature of evidence and indicators was weighted according to [Table 6.1](#).

A hypothesis was then established that considered the database of ground evidence for sites that have been sampled, but occurrences of gas hydrates might not be restricted to these point locations. If a given pixel were located between a ground evidence and an indicator, the likeliness of that pixel containing gas hydrates would be greater than that of a pixel located far from either. Given the discrete nature of the features described within the database and the relative concept of this likeliness, a regionalization technique was applied following a smoothed saturated algorithm of kernel density. Here, the weighting of the features represents an abstract concept of the confidence of having gas hydrates. This technique consists of a kernel density estimation, which fits a smoothly tapered surface to each point or polyline. The search radius (default option) was calculated on the basis of the spatial configuration and the number of input points. This approach corrects for spatial outliers (input points that are very far from the rest), so they will not make the search radius unreasonably large. These values of the weighted density map were then normalized from zero to one ([Fig. 6.2](#)) to remove the per area output of the model, providing a relative likeliness of between 0 and 1, where 0 means that there is very little (but not no) confidence of finding significant amounts of gas hydrates at that location and 1 means that there is certainty of finding gas hydrates at that location.



Map of the GHSZ on the seafloor

The map of the theoretical GHSZ for gases of biogenic origin of Núñez-Varela (2020) was zoned into three sectors according to the pressure (bathymetry)/temperature conditions: unstable areas, stable areas and a strip (from 0 to 50 m in thickness) at the base of the GHSZ where hydrate stability is extremely weak (Fig. 6.1). The base of the GHSZ in the vicinity of the low-latitude Atlantic Ocean volcanic islands (e.g. the Azores, Madeira and the Canary Islands) was not taken into account owing to the absence of hydrocarbon reservoirs at these geological sites.

Finally, this map was weighted in relation to the mean value of the normalized density map of evidence and indicators.

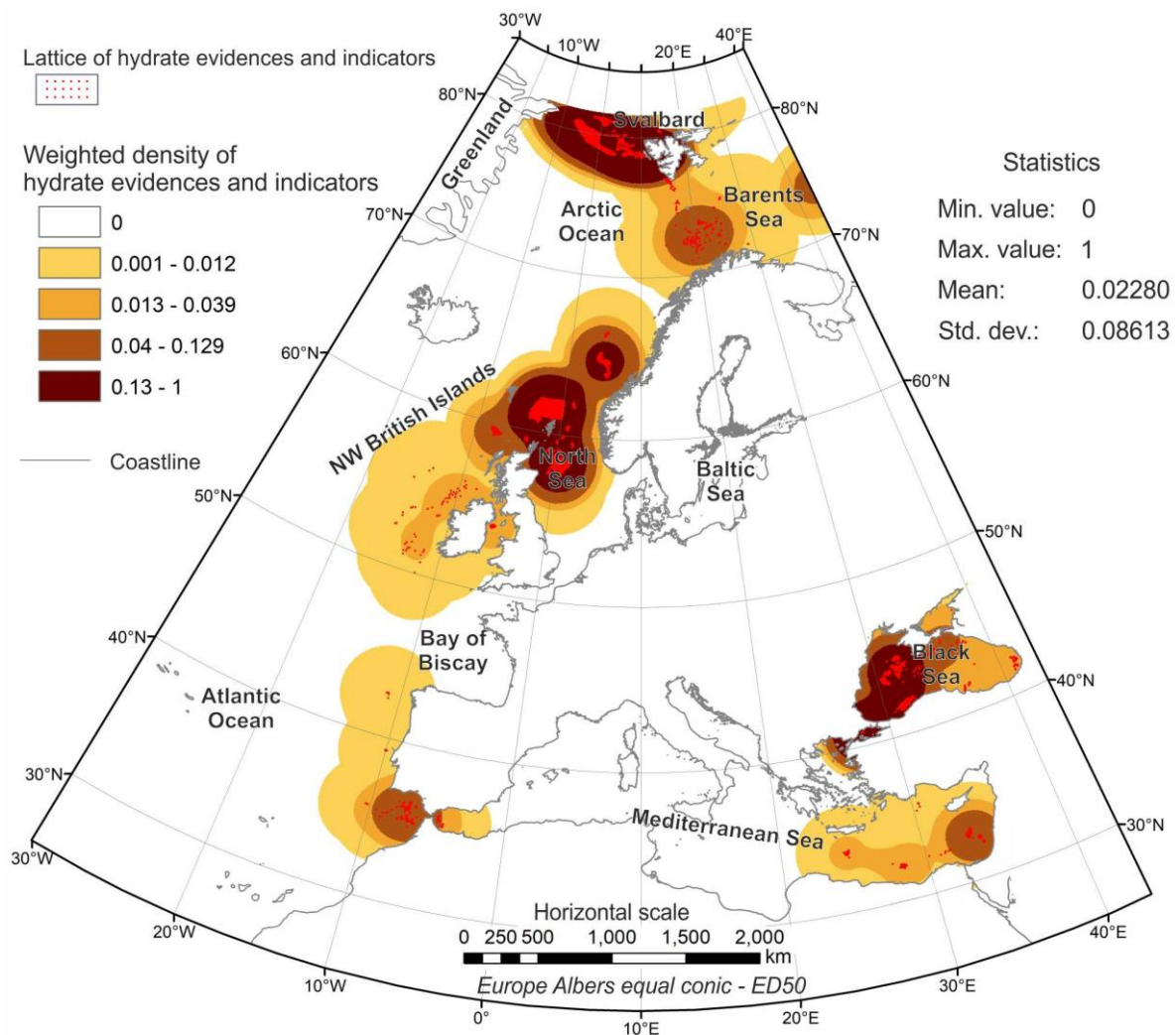


Fig. 6.2. Density map of gas hydrate evidence and indicators.



Susceptibility map

The susceptibility was assessed by map algebra, taking into account the control maps of density of hydrate evidences and indicators and the weighted map of the GHSZ on the seafloor. Specifically, the final map (Fig. 6.3) was conceived as a segmentation in three levels by quantiles resulting from the addition of the above control maps:

$$Sc = \delta_{ei} + GHSZ_w$$

where Sc , is the susceptibility map; δ_{ei} , is the normalized weighted density map of hydrate evidences and indicators; and $GHSZ_w$, is the weighted map of the GHSZ on the seafloor

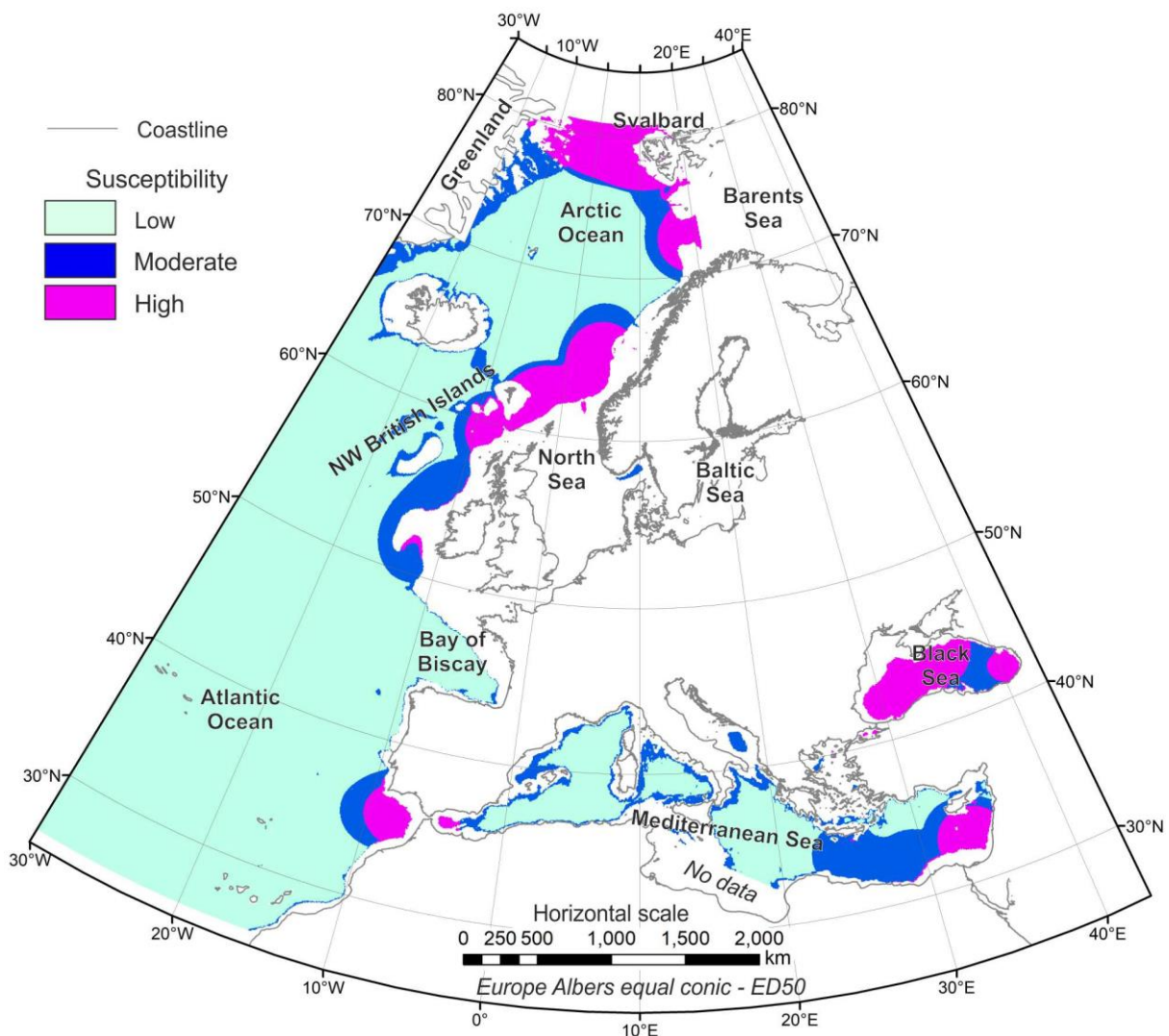


Fig. 6.3. Assessment of susceptibility of the seafloor to being affected by gas hydrate dissociation processes.



6.1. Discussion

Because of the methodology applied, the susceptibility map shows low values in areas that have knowledge gaps or have been poorly surveyed. This inevitably leads to two interpretations: (i) the catalogue is incomplete, these areas have been poorly surveyed, no records have been recovered, but hydrates may exist and subsequently a high susceptibility may be potentially latent; and (ii) there are no data because there is no evidence or indicators of hydrates. These knowledge gaps could be especially critical at the base of the GHSZ. Particularly on the east Greenland shelf, the Irish margin, the western Iberian margin and the Mediterranean Sea, no hydrates have been recovered but hydrocarbon seabed fluid flow structures or seismic indicators (e.g. on the Irish margin) have been observed.

The majority of gas hydrate evidence stored in the database was recovered in focused seabed fluid flow structures such as mud volcanoes or pockmarks. This is especially significant in the southern European margins such as the Gulf of Cádiz and the western Mediterranean Sea. In these cases, gas hydrates are circumscribed to the feeder systems of the hydrocarbon fluid migration structures which, subject to certain exceptions, do not exceed 0.1 to 1 km and 4 km in diameter for pockmarks and mud volcanoes, respectively. In these areas, there is therefore no continuous spatial variation of the presence of hydrates. Gas hydrates appear with a located distribution (the nugget effect?) and are focused inside the hydrocarbon fluid flow structures, where fluid migration is mainly controlled by faults. Nevertheless, the presence of hydrocarbon fluid flow structures shows a continuous spatial variation in fluid leakage areas. In these areas, the density map indicates areas where hydrate-bearing fluid flow structures are more likely, and subsequently the likelihood of the seafloor suffering gas hydrate dissociation processes caused by natural or human activities could also be high. Finally, although the susceptibility could be high in mud volcano fields, for instance, the real risk of dissociation processes, or their magnitude, will be low due to the type or internal structure of the hydrates inside the sediment. In mud volcanoes, hydrates constitute small crystals or aggregates (measuring millimetres or centimetres) and their real volume is low.

The future scenario of global warming projected by the scientific community ([Gillett, 2015](#); [Schmittner et al., 2005](#); [Vellinga and Wood, 2002](#)) increases the susceptibility assessed by the direct effect of the ocean temperature increase on gas hydrate stability ([Ketzer et al., 2020](#)) and the isostatic rebound in polar and sub-polar areas ([Wallmann et al., 2018](#)). This direct effect (a seafloor temperature increase and an effective seafloor pressure decrease) will have a high impact on the east Greenland shelf, the northwest Norwegian margin, Svalbard and the Barents Sea, and the susceptibility of these areas will thus increase greatly. Furthermore, future changes in the thermohaline circulation ([Schmittner et al., 2005](#); [Vellinga and Wood, 2002](#)) could have dramatic effects on the seafloor temperature and subsequently on hydrate stability at high latitudes.



7. CONCLUSIONS

- In order to a fully interoperability of the hydrate related information, future hydrate related data should be collected and stored compliant the data model structure of the hydrate GIS-data base of GARAH project. Particularly, the four groups of items (location, property metadata, geo-descriptors and references) should be filled according to the standards applied on it.
- Geological and geophysical evidence and indicators of the presence of marine gas hydrates and the oceanographic variables controlling the GHSZ show a heterogeneous distribution and knowledge gaps (areas with <1 record per 100 km²) along the European continental margins. Some of these knowledge gaps have been classified as critical: (i) for geothermal gradient, data on the east of Greenland, Svalbard, the northern Norwegian margin, the southern Barents Sea and the White Sea, the north of the British Islands, the Gulf of Cádiz, the Bay of Biscay, the north-western Iberian margin and the southwestern Mediterranean Sea; and (ii) for seafloor temperature/salinity data on east of Greenland, the western Barents Sea and White Sea, the northern Black Sea and the south-eastern Mediterranean Sea.
- Taking into account the critical knowledge gaps, the theoretical thickness of the GHSZ and the density of records of hydrate evidence and indicators, oceanographic parameters (geothermal gradient, seafloor temperature and salinity) and seabed fluid flow structures, nine areas of interest for future scientific projects were defined: east Greenland and Svalbard, the west Barents and White seas, the northwest Norwegian margin, the northwest British Islands, the Bay of Biscay and the northwest Iberian margin, the southern Iberian and northern Moroccan margins, the Tunisian and Libyan margins, the eastern Mediterranean, and the Black and Marmara seas.
- In the Bay of Biscay, an estimation for potential safe CO₂ deep offshore storage capacity has been developed. French EEZ storage volume estimate of 3,422 km³ is of the same order of magnitude as the total storage volume in the Spanish EEZ estimate of 3,700 km³. There is, however, a big difference resulting from the seafloor depth: in the French case, almost all the stored volume is occupied by gas hydrates, whereas in the Spanish case, about the half (1,728 km³) is occupied by CO₂ in hydrate phase and the other half (1,972 km³) by liquid CO₂.
- The susceptibility assessment of occurrence of hydrate dissociation processes on the seafloor shows high values in Svalbard, the northern Norwegian margin—Barents Sea, the continental slope of the mid-Norwegian margin and the North Sea, the Gulf of Cádiz and the eastern Mediterranean and the Black Sea. Moderate values are observed on the continental shelf of western Greenland, the northwest of the British Islands and the continental slope of the western and northern Mediterranean Sea.



8. REFERENCES

Akhmetzhanov, A.M., Ivanov, M.K., Kenyon, N.H., Mazzini, A., 2007. Deep-water Cold Seeps, Sedimentary Environments and Ecosystems of the Black and Tyrrhenian Seas and the Gulf of Cadiz: Preliminary Results of Investigations During the TTR-15 Cruise of RV Professor Logachev, June-August, 2005, IOC Technical Series. Unesco, United Nations Educational, Paris.

Akhmetzhanov, A.M., Kenyon, N.H., Ivanov, M.K., Westbrook, G., Mazzini, A., 2008. Deep-water depositional systems and cold seeps of the Western Mediterranean, Gulf of Cadiz and Norwegian continental margins. Preliminary results of investigations during the TTR-16 cruise of RV Professor Logachev, May-July, 2006. Technical Series. Intergovernmental Oceanographic Commission = Série technique.

Alazard-toux, N., Criqui, P., Devezeaux de Lavergne et al., 2015. Decarbonization Wedges. ANCRE. <http://www.allianceenergie.fr>

Aloisi, G., Pierre, C., Rouchy, J.-M., Foucher, J.-P., Woodside, J., 2000. Methane-related authigenic carbonates of eastern Mediterranean Sea mud volcanoes and their possible relation to gas hydrate destabilisation. *Earth and Planetary Science Letters* 184, 321–338. [https://doi.org/10.1016/S0012-821X\(00\)00322-8](https://doi.org/10.1016/S0012-821X(00)00322-8)

Archer, D. E., Morford, J. L., & Emerson, S. R. 2002. A model of suboxic sedimentary diagenesis suitable for automatic tuning and gridded global domains. *Global Biogeochemical Cycles*, 16(1), 17-1.

Behrenfeld, M. J., & Falkowski, P. G. 1997. Photosynthetic rates derived from satellite-based chlorophyll concentration. *Limnology and oceanography*, 42(1), 1-20.

Bernardino, A.F., Levin, L.A., Thurber, A.R., Smith, C.R., 2012. Comparative Composition, Diversity and Trophic Ecology of Sediment Macrofauna at Vents, Seeps and Organic Falls. *PLOS ONE* 7, e33515. <https://doi.org/10.1371/journal.pone.0033515>

Betlem, P., Senger, K., Hodson, A., 2019. 3D thermobaric modelling of the gas hydrate stability zone onshore central Spitsbergen, Arctic Norway. *Marine and Petroleum Geology* 100, 246–262. <https://doi.org/10.1016/j.marpetgeo.2018.10.050>

Boswell, R., Yamamoto, K., Lee, S.-R., Collett, T., Kumar, P., Dallimore, S., 2014. Chapter 8 - Methane Hydrates, in: Letcher, T.M. (Ed.), *Future Energy (Second Edition)*. Elsevier, Boston, pp. 159–178. <https://doi.org/10.1016/B978-0-08-099424-6.00008-9>

Bouriak, S., Vanneste, M., Saoutkine, A., 2000. Inferred gas hydrates and clay diapirs near the Storegga Slide on the southern edge of the Vøring Plateau, offshore Norway. *Marine Geology* 163, 125–148. [https://doi.org/10.1016/S0025-3227\(99\)00115-2](https://doi.org/10.1016/S0025-3227(99)00115-2)

Bourry, C., Chazallon, B., Charlou, J.L., Pierre Donval, J., Ruffine, L., Henry, P., Geli, L., Çagatay, M.N., İnan, S., Moreau, M., 2009. Free gas and gas hydrates from the Sea of Marmara, Turkey: Chemical and structural characterization. *Chemical Geology* 264, 197–206. <https://doi.org/10.1016/j.chemgeo.2009.03.007>

Bugge, T., Belderson, R.H., Kenyon, N.H., Falcon, N.L., 1988. The Storegga slide. *Philosophical Transactions of the Royal Society of London. Series A, Mathematical and Physical Sciences* 325, 357–388. <https://doi.org/10.1098/rsta.1988.0055>

Bünz, S., Mienert, J., Berndt, C., 2003. Geological controls on the Storegga gas-hydrate system of the mid-Norwegian continental margin. *Earth and Planetary Science Letters* 209, 291–307. [https://doi.org/10.1016/S0012-821X\(03\)00097-9](https://doi.org/10.1016/S0012-821X(03)00097-9)

Burnol, A., Thinon, I., Ruffine, L., et al, 2015. Influence of impurities (nitrogen and methane) on the CO₂ storage capacity as sediment-hosted gas hydrates – application in the area of the Celtic Sea and the Bay of Biscay. *International Journal of Greenhouse Gas Control*, vol. 35, pp. 96–109. <https://doi.org/10.1016/j.ijggc.2015.01.018>

Burnol, A., 2018. Roles of Gas Hydrates for CO₂ Geological Storage Purposes, in: Ruffine, L., Broseta, D., Desmedt, A. (Eds.), *Gas Hydrates 2*. John Wiley & Sons, Inc., Hoboken, NJ, USA, pp. 267–284. <https://doi.org/10.1002/9781119451174.ch13>



- Clark, P.U., Pisias, N.G., Stocker, T.F., Weaver, A.J., 2002. The role of the thermohaline circulation in abrupt climate change. *Nature* 415, 863–869. <https://doi.org/10.1038/415863a>
- Cordes, E.E., Bergquist, D.C., Fisher, C.R., 2009. Macro-Ecology of Gulf of Mexico Cold Seeps. *Annual Review of Marine Science* 1, 143–168. <https://doi.org/10.1146/annurev.marine.010908.163912>
- Daniels, C. J., Poulton, A. J., Balch, W. M., Marañón, E., Adey, T., Bowler, B. C., & Feng, Y. (2018). A global compilation of coccolithophore calcification rates. *Earth System Science Data*, 10(4), 1859–1876.
- Davie, M. K., & Buffett, B. A. 2001. A numerical model for the formation of gas hydrate below the seafloor. *Journal of Geophysical Research: Solid Earth*, 106(B1), 497–514
- De Lange, G.J., Brumsack, H.-J., 1998a. Pore-water indications for the occurrence of gas hydrates in eastern Mediterranean mud dome structures. *Proceedings of the Ocean Drilling Program: Scientific Results* 160, 569–574.
- De Lange, G.J., Brumsack, H.-J., 1998b. The occurrence of gas hydrates in Eastern Mediterranean mud dome structures as indicated by pore-water composition. *Geological Society, London, Special Publications* 137, 167–175. <https://doi.org/10.1144/GSL.SP.1998.137.01.14>
- Depreiter, D., Poort, J., Rensbergen, P.V., Henriët, J.P., 2005. Geophysical evidence of gas hydrates in shallow submarine mud volcanoes on the Moroccan margin. *Journal of Geophysical Research: Solid Earth* 110. <https://doi.org/10.1029/2005JB003622>.
- De Visser, E., Hendriks, C., Barrio, M., Mølnvik, M. J., de Koeijer, G., Liljemark, S., & Le Gallo, Y. (2008). Dynamis CO2 quality recommendations. *International journal of greenhouse gas control*, 2(4), 478–484. <https://doi.org/10.1016/j.ijggc.2008.04.006>
- Díaz-del-Río, V., Somoza, L., Martínez-Frias, J., Mata, M.P., Delgado, A., Hernandez-Molina, F.J., Lunar, R., Martín-Rubí, J.A., Maestro, A., Fernández-Puga, M.C., León, R., Llave, E., Medialdea, T., Vázquez, J.T., 2003. Vast fields of hydrocarbon-derived carbonate chimneys related to the accretionary wedge/olistostrome of the Gulf of Cádiz. *Marine Geology* 195, 177–200. [https://doi.org/10.1016/S0025-3227\(02\)00687-4](https://doi.org/10.1016/S0025-3227(02)00687-4).
- Dickens, G.R., 2003. Rethinking the global carbon cycle with a large, dynamic and microbially mediated gas hydrate capacitor. *Earth and Planetary Science Letters* 213, 169–183. [https://doi.org/10.1016/S0012-821X\(03\)00325-X](https://doi.org/10.1016/S0012-821X(03)00325-X)
- Dickens, G.R., 2001. The potential volume of oceanic methane hydrates with variable external conditions. *Organic Geochemistry* 32, 1179–1193. [https://doi.org/10.1016/S0146-6380\(01\)00086-9](https://doi.org/10.1016/S0146-6380(01)00086-9)
- Eccles, J.K., Pratson, L., 2013. Economic evaluation of offshore storage potential in the US Exclusive Economic Zone, *Greenhouse Gases: Science and Technology*. vol. 3, pp. 84–95, 2013. <https://doi.org/10.1002/ghg.1308>
- Egorov, V.N., Artemov, Y.G., Gulín, S.B., Gennadiy, P., G.G., 2011. Methane seeps in the Black Sea: discovery, quantification and environmental assessment. *J. Black Sea/Mediterranean Environ.* 17, 171–185.
- EMODnet Bathymetry [WWW Document], n.d. URL <https://www.emodnet-bathymetry.eu/> (accessed 11.10.20).
- Foucher, J.-P., Westbrook, G., Boëtius, A., Ceramicola, S., Dupré, S., Mascle, J., Mienert, J., Pfannkuche, O., Pierre, C., Praeg, D., 2009. Structure and Drivers of Cold Seep Ecosystems. *Oceanography* 22, 92–109.
- Gillett, N.P., 2015. Weighting climate model projections using observational constraints. *Philosophical Transactions of the Royal Society A: Mathematical, Physical and Engineering Sciences* 373, 20140425. <https://doi.org/10.1098/rsta.2014.0425>
- Ginsburg, G.D., Milkov, A.V., Soloviev, V.A., Egorov, A.V., Cherkashev, G.A., Vogt, P.R., Crane, K., Lorenson, T.D., Khutorskoy, M.D., 1999. Gas hydrate accumulation at the Hakon Mosby Mud Volcano. *Geo-Marine Letters* 19, 57–67. <https://doi.org/10.1007/s003670050093>
- Hensen, C., Scholz, F., Nuzzo, M., Valadares, V., Gràcia, E., Terrinha, P., Liebetrau, V., Kaul, N., Silva, S., Martínez-Loriente, S., Bartolome, R., Piñero, E., Magalhães, V.H., Schmidt, M., Weise, S.M., Cunha, M., Hilario, A., Perea, H., Rovelli, L., Lackschewitz, K., 2015. Strike-slip faults mediate the rise of



crustal-derived fluids and mud volcanism in the deep sea. *Geology* 43, 339–342. <https://doi.org/10.1130/G36359.1>

Hernández-Molina, F.J., Serra, N., Stow, D.A.V., Llave, E., Ercilla, G., Van Rooij, D., 2011. Along-slope oceanographic processes and sedimentary products around the Iberian margin. *Geo-Mar Lett* 31, 315–341. <https://doi.org/10.1007/s00367-011-0242-2>

Hopper, J.R., Funck, T., Stoker, M., Arting, U., Peron-Pinvidic, G., Doornenbal, H., Gaina, C., 2014. Tectonostratigraphic atlas of the North-East Atlantic region. Geological Survey of Denmark and Greenland, Copenhagen, Denmark.

House, K.Z., Schrag, D.P., Harvey, C.F. et al., 2006. Permanent carbon dioxide storage in deep-sea sediments. *Proceedings of the National Academy of Sciences*, vol. 103, pp. 12291–12295. <https://doi.org/10.1073/pnas.0605318103>

Ivanov, M.K., Kenyon, N.H., Laberg, J.S., Blinova, N.B., 2010. Cold seeps, coral mounds and deepwater depositional systems of the Alboran Sea, Gulf of Cadiz and Norwegian continental margin. Preliminary results of investigations during the TTR-17 cruise of RV Professor Logachev, May-July, 2008, IOC Technical Series. Unesco, United Nations Educational, Paris.

Johnson, J.E., Mienert, J., Plaza-Faverola, A., Vadakkepulyambatta, S., Knies, J., Bünz, S., Andreassen, K., Ferré, B., 2015. Abiotic methane from ultraslow-spreading ridges can charge Arctic gas hydrates. *Geology* 43, 371–374. <https://doi.org/10.1130/G36440.1>

Kenyon, N.H., Ivanov, M.K., Akhmetzhanov, A.M., Akhmanov, G.G., 2002. Geological processes in the Mediterranean and Black Seas and North East Atlantic. Preliminary results of investigations during the TTR-11 cruise of RV Professor Logachov July-September, 2001. Technical Series. Intergovernmental Oceanographic Commission = Série technique.

Kenyon, N.H., Ivanov, M.K., Akhmetzhanov, A.M., Akhmanov, G.G., 2001. Interdisciplinary Approaches to Geoscience on the North East Atlantic Margin and Mid-Atlantic Ridge: Preliminary Results of Investigations During the TTR-10 Cruise of RV Professor Logachev, July-September 2000, IOC Technical Series. Unesco, United Nations Educational, Paris.

Kenyon, N.H., Ivanov, M.K., Akhmetzhanov, A.M., Akhmanov, G.G., 2000. Multidisciplinary Study of Geological Processes on the North East Atlantic and Western Mediterranean Margins: Preliminary Results of Geological and Geophysical Investigations During the TTR-9 Cruise of R/V Professor Logachev June-July, 1999, IOC Technical Series. Unesco, United Nations Educational, Paris.

Kenyon, N.H., Ivanov, M.K., Akhmetzhanov, A.M., Kozlova, E.V., 2006. Interdisciplinary geoscience studies of the Gulf of Cadiz and Western Mediterranean basins: Preliminary results of investigations during the TTR-14 cruise of RV Professor Logachev, July-September, 2004, IOC Technical Series. Unesco, United Nations Educational, Paris.

Kenyon, N.H., Ivanov, M.K., Akhmetzhanov, A.M., Kozlova, E.V., Mazzini, A., 2004. Interdisciplinary studies of North Atlantic and Labrador Sea margin architecture and sedimentary processes. Preliminary results of investigations during the TTR-13 cruise of RV Professor Logachev, July-September, 2003, IOC Technical Series. Unesco, United Nations Educational, Paris.

Ketzer, M., Praeg, D., Rodrigues, L.F., Augustin, A., Pivel, M.A.G., Rahmati-Abkenar, M., Miller, D.J., Viana, A.R., Cupertino, J.A., 2020. Gas hydrate dissociation linked to contemporary ocean warming in the southern hemisphere. *Nat Commun* 11, 3788. <https://doi.org/10.1038/s41467-020-17289-z>

Koide, H., Takahashi, M., Tsukamoto, H. et al., 1995. Self-trapping mechanisms of carbon dioxide in the aquifer disposal. *Energy Conversion and Management*, vol. 36, pp. 505–508. [https://doi.org/10.1016/0196-8904\(95\)00054-H](https://doi.org/10.1016/0196-8904(95)00054-H)

Kopf, A., Bannert, B., Brückmann, W., Dorschel, B., Foubert, A.T.G., Grevemeyer, I., Gutscher, M.-A., Hebbeln, D., Heesemann, B., Hensen, C., Kaul, N.E., Lutz, M., Magalhaes, V.H. da S., Marquardt, M.J., Marti, A.V., Nass, K.S., Neubert, N., Niemann, H., Nuzzo, M., Poort, J.P.D., Rosiak, U.D., Sahling, H., Schneider von Deimling, J., Somoza Losada, L., Thiebot, E., Wilkop, T.P., 2004. Report and preliminary results of SONNE cruise SO175, Miami - Bremerhaven, 12.11 - 30.12.2003 : (GAP, Gibraltar Arc Processes) (Report), *Berichte aus dem Fachbereich Geowissenschaften der Universität Bremen*, 228pp.



- Kunz, O., Wagner, W., 2012. The GERG-2008 wide-range equation of state for natural gases and other mixtures: an expansion of GERG-2004. *Journal of Chemical & Engineering Data*, vol. 57, pp. 3032–3091. <https://doi.org/10.1021/je300655b>
- Kvenvolden, K.A., 1988. Methane hydrate — A major reservoir of carbon in the shallow geosphere? *Chemical Geology* 71, 41–51. [https://doi.org/10.1016/0009-2541\(88\)90104-0](https://doi.org/10.1016/0009-2541(88)90104-0)
- Kvenvolden, K.A. 1995 A review of the geochemistry of methane in natural gas hydrate, *Org. Geochem.* 23: 997 - 1008
- Laberg, J.S., Andreassen, K., Knutsen, S.-M., 1998. Inferred gas hydrate on the Barents Sea shelf - A model for its formation and a volume estimate. *Geo-Marine Letters* 18, 26–33. <https://doi.org/10.1007/s003670050048>
- León, R., Somoza, L., Medialdea, T., Maestro, A., Díaz-del-Río, V., Fernández-Puga, M. del C., 2006. Classification of sea-floor features associated with methane seeps along the Gulf of Cádiz continental margin. *Deep Sea Research Part II: Topical Studies in Oceanography* 53, 1464–1481. <https://doi.org/10.1016/j.dsr2.2006.04.009>
- León, R., Somoza, L., Giménez-Moreno, C.J., Dabrio, C.J., Ercilla, G., Praeg, D., Díaz-del-Río, V., Gómez-Delgado, M., 2009. A predictive numerical model for potential mapping of the gas hydrate stability zone in the Gulf of Cadiz. *Marine and Petroleum Geology* 26, 1564–1579. <https://doi.org/10.1016/j.marpetgeo.2009.01.016>
- León, R., Somoza, L., Medialdea, T., Hernández-Molina, F.J., Vázquez, J.T., Díaz-del-Río, V., González, F.J., 2010. Pockmarks, collapses and blind valleys in the Gulf of Cádiz. *Geo-Mar Lett* 30, 231–247. <https://doi.org/10.1007/s00367-009-0169-z>
- León, R., Somoza, L., Medialdea, T., Vázquez, J.T., González, F.J., López-González, N., Casas, D., del Pilar Mata, M., del Fernández-Puga, M.C., Giménez-Moreno, C.J., Díaz-del-Río, V., 2012. New discoveries of mud volcanoes on the Moroccan Atlantic continental margin (Gulf of Cádiz): morpho-structural characterization. *Geo-Mar Lett* 32, 473–488. <https://doi.org/10.1007/s00367-012-0275-1>
- Levine, J.S., Matter, J.M., Goldberg, D. et al., 2007. Gravitational trapping of carbon dioxide in deep sea sediments: Permeability, buoyancy, and geomechanical analysis. *Geophysical Research Letters*, vol. 34, p. L24703. <https://doi.org/10.1029/2007GL031560>
- Lykousis, V., Alexandri, S., Woodside, J., de Lange, G., Dähmann, A., Perissoratis, C., Heeschen, K., Ioakim, Chr., Sakellariou, D., Nomikou, P., Rousakis, G., Casas, D., Ballas, D., Ercilla, G., 2009. Mud volcanoes and gas hydrates in the Anaximander mountains (Eastern Mediterranean Sea). *Marine and Petroleum Geology* 26, 854–872. <https://doi.org/10.1016/j.marpetgeo.2008.05.002>
- Magalhães, V.H., Pinheiro, L.M., Ivanov, M.K., Kozlova, E., Blinova, V., Kolganova, J., Vasconcelos, C., McKenzie, J.A., Bernasconi, S.M., Kopf, A.J., Díaz-del-Río, V., González, F.J., Somoza, L., 2012. Formation processes of methane-derived authigenic carbonates from the Gulf of Cadiz. *Sedimentary Geology* 243–244, 155–168. <https://doi.org/10.1016/j.sedgeo.2011.10.013>
- Masclé, J., Mary, F., Praeg, D., Brosolo, L., Camera, L., Ceramicola, S., Dupré, S., 2014. Distribution and geological control of mud volcanoes and other fluid/free gas seepage features in the Mediterranean Sea and nearby Gulf of Cadiz. *Geo-Mar Lett* 34, 89–110. <https://doi.org/10.1007/s00367-014-0356-4>
- Maslin, M., Owen, M., Betts, R., Day, S., Dunkley Jones, T., Ridgwell, A., 2010. Gas hydrates: past and future geohazard? *Philosophical Transactions of the Royal Society A: Mathematical, Physical and Engineering Sciences* 368, 2369–2393. <https://doi.org/10.1098/rsta.2010.0065>
- McConnell, D.R., Zhang, Z., Boswell, R., 2012. Review of progress in evaluating gas hydrate drilling hazards. *Marine and Petroleum Geology, Resource and hazard implications of gas hydrates in the Northern Gulf of Mexico: Results of the 2009 Joint Industry Project Leg II Drilling Expedition* 34, 209–223. <https://doi.org/10.1016/j.marpetgeo.2012.02.010>
- Mikkelsen, N., Laier, T., Nielsen, T., Kuijpers, A., Nørgaard-Pedersen, N., 2012. Methane and possible gas hydrates in the Disko Bugt region, central West Greenland. *GEUS Bulletin* 26, 69–72. <https://doi.org/10.34194/geusb.v26.4764>



Minshull, T.A., Marín-Moreno, H., Betlem, P., Bialas, J., Bünz, S., Burwicz, E., Cameselle, A.L., Cifci, G., Giustiniani, M., Hillman, J.I.T., Hölz, S., Hopper, J.R., Ion, G., León, R., Magalhaes, V., Makovsky, Y., Mata, M.-P., Max, M.D., Nielsen, T., Okay, S., Ostrovsky, I., O'Neill, N., Pinheiro, L.M., Plaza-Faverola, A.A., Rey, D., Roy, S., Schwalenberg, K., Senger, K., Vadakkepuliymbatta, S., Vasilev, A., Vázquez, J.-T., 2020. Hydrate occurrence in Europe: A review of available evidence. *Marine and Petroleum Geology* 111, 735–764. <https://doi.org/10.1016/j.marpetgeo.2019.08.014>

Mazurenko, L.L., Soloviev, V.A., Belenkaya, I., Ivanov, M.K., Pinheiro, L.M., 2002. Mud volcano gas hydrates in the Gulf of Cadiz. *Terra. Nova* 14, 321–329.

Nielsen, T., Laier, T., Mikkelsen, N. & Kristensen, J.B. 2011: Permagas project: Sampling gas hydrates in the Disko Bay area. Cruise Report – R/V Paamiut 20 to 26 June 2011. Danmarks og Grønlands Geologiske Undersøgelser Rapport 2011/105, 40 pp

Nielsen, T., Laier, T., Kuijpers, A., Rasmussen, T.L., Mikkelsen, N.E., Nørgård-Pedersen, N., 2014. Fluid flow and methane occurrences in the Disko Bugt area offshore West Greenland: indications for gas hydrates? *Geo-Mar Lett* 34, 511–523. <https://doi.org/10.1007/s00367-014-0382-2>

Núñez-Varela, E., 2020. Cálculo del campo teórico de la zona de estabilidad de los hidratos de gas natural biogénico en los márgenes continentales europeos. *Open_igme VII*, 85. <http://hdl.handle.net/20.500.12468/679>

Pape, T., Kasten, S., Zabel, M., Bahr, A., Abegg, F., Hohnberg, H.-J., Bohrmann, G., 2010. Gas hydrates in shallow deposits of the Amsterdam mud volcano, Anaximander Mountains, Northeastern Mediterranean Sea. *Geo-Mar Lett* 30, 187–206. <https://doi.org/10.1007/s00367-010-0197-8>

Paull, C.K., Dallimore, S.R., Caress, D.W., Gwiazda, R., Melling, H., Riedel, M., Jin, Y.K., Hong, J.K., Kim, Y.-G., Graves, D., Sherman, A., Lundsten, E., Anderson, K., Lundsten, L., Villinger, H., Kopf, A., Johnson, S.B., Clarke, J.H., Blasco, S., Conway, K., Neelands, P., Thomas, H., Côté, M., 2015. Active mud volcanoes on the continental slope of the Canadian Beaufort Sea. *Geochemistry, Geophysics, Geosystems* 16, 3160–3181. <https://doi.org/10.1002/2015GC005928>

Petrov O.V., Morozov A.F., Zastrozhnov A.S., Shkatova V.K., Minina E.A., Tarnogradsky V.D., Astakhov V.I., Ryzhkova V.M., Chuiko M.A., Yakovleva S.B., Zhuravleva O.Yu., Pestova L.E., Snezhko O.N., Gusev E.A., Sheiko A.A. 2019. Map of Quaternary Formations of the Russian Federation and Adjacent Deep Water Areas. Eds. Russian Geological Research Institute (VSEGEI). Petrov O.V., Morozov A.F., Zastrozhnov A.S., Shkatova V.K., Minina E.A., Tarnogradsky V.D., Astakhov V.I., Ryzhkova V.M., Chuiko M.A., Yakovleva S.B., Zhuravleva O.Yu., Pestova L.E., Snezhko O.N., Gusev E.A., Sheiko A.A. 2019. Map of Quaternary Formations of the Russian Federation and Adjacent Deep Water Areas. Eds. Russian Geological Research Institute (VSEGEI). <https://vsegei.ru/en/about/news/99861/>

Piñero, E., Marquardt, M., Hensen, C., Haecel, M., Wallmann, K., 2013. Estimation of the global inventory of methane hydrates in marine sediments using transfer functions. *Biogeosciences* 10, 959–975. <https://doi.org/10.5194/bg-10-959-2013>

Plaza-Faverola, A., Bünz, S., Johnson, J.E., Chand, S., Knies, J., Mienert, J., Franek, P., 2015. Role of tectonic stress in seepage evolution along the gas hydrate-charged Vestnesa Ridge, Fram Strait. *Geophysical Research Letters* 42, 733–742. <https://doi.org/10.1002/2014GL062474>

Plaza-Faverola, A., Vadakkepuliymbatta, S., Hong, W.-L., Mienert, J., Bünz, S., Chand, S., Greinert, J., 2017. Bottom-simulating reflector dynamics at Arctic thermogenic gas provinces: An example from Vestnesa Ridge, offshore west Svalbard. *Journal of Geophysical Research: Solid Earth* 122, 4089–4105. <https://doi.org/10.1002/2016JB013761>

Popescu, I., Lericolais, G., Panin, N., De Batist, M., Gillet, H., 2007. Seismic expression of gas and gas hydrates across the western Black Sea. *Geo-Mar Lett* 27, 173–183. <https://doi.org/10.1007/s00367-007-0068-0>

Posewang, J., Mienert, J., 1999. The enigma of double BSRs: Indicators for changes in the hydrate stability field? *Geo-Marine Letters* 19, 157–163. <https://doi.org/10.1007/s003670050103>

Reeburgh, W.S., 2007. Oceanic Methane Biogeochemistry. *Chem. Rev.* 107, 486–513. <https://doi.org/10.1021/cr050362v>



- Riboulot, V., Ker, S., Sultan, N., Thomas, Y., Marsset, B., Scalabrin, C., Ruffine, L., Boulart, C., Ion, G., 2018. Freshwater lake to salt-water sea causing widespread hydrate dissociation in the Black Sea. *Nature Communications* 9, 117. <https://doi.org/10.1038/s41467-017-02271-z>
- Ristova, P.P., Wenzhöfer, F., Ramette, A., Felden, J., Boetius, A., 2015. Spatial scales of bacterial community diversity at cold seeps (Eastern Mediterranean Sea). *The ISME Journal* 9, 1306–1318. <https://doi.org/10.1038/ismej.2014.217>
- Rochelle, C.A., Camps, A.P., Long, D. et al., 2009. Can CO₂ hydrate assist in the underground storage of carbon dioxide?. *Geological Society, London, Special Publications*, vol. 319, pp. 171–183. <https://doi.org/10.1144/SP319.14>
- Römer, M., Sahling, H., Pape, T., dos Santos Ferreira, C., Wenzhöfer, F., Boetius, A., Bohrmann, G., 2014. Methane fluxes and carbonate deposits at a cold seep area of the Central Nile Deep Sea Fan, Eastern Mediterranean Sea. *Marine Geology* 347, 27–42. <https://doi.org/10.1016/j.margeo.2013.10.011>
- Roy, S., Marin-Moreno, H., Max, M.D., 2017. Natural Gas Hydrates and fluid flow: implications from Irish offshore. In: 9th International Conference on Gas Hydrates, Denver, Colorado, USA.
- Roy, S., Max, M.D., Walsh, J., 2018. Assessment of Natural Gas Hydrate Petroleum System in western Irish offshore. *AGU Fall Meeting Abstracts* 51.
- Saunders, P.M., 1981. Practical conversion of pressure to depth. *Journal of Physical Oceanography*, vol. 11, pp. 573–574. [https://doi.org/10.1175/1520-0485\(1981\)011<0573:PCOPTD>2.0.CO;2](https://doi.org/10.1175/1520-0485(1981)011<0573:PCOPTD>2.0.CO;2)
- Shakhova, N., Semiletov, I., Leifer, I., Sergienko, V., Salyuk, A., Kosmach, D., Chernykh, D., Stubbs, C., Nicolsky, D., Tumskoy, V., Gustafsson, Ö., 2014. Ebullition and storm-induced methane release from the East Siberian Arctic Shelf. *Nature Geoscience* 7, 64–70. <https://doi.org/10.1038/ngeo2007>
- Senger, K., Bünz, S., Mienert, J., 2010. First-Order Estimation of In-Place Gas Resources at the Nyegga Gas Hydrate Prospect, Norwegian Sea. *Energies* 3, 2001–2026. <https://doi.org/10.3390/en3122001>
- Serov, P., Vadakkepuliymbatta, S., Mienert, J., Patton, H., Portnov, A., Silyakova, A., Panieri, G., Carroll, M.L., Carroll, J., Andreassen, K., Hubbard, A. 2017. Postglacial response of Arctic Ocean gas hydrates to climatic amelioration. *PNAS* 114, 6215–6220. <https://doi.org/10.1073/pnas.1619288114>
- Sloan, E.D., 2003. Fundamental principles and applications of natural gas hydrates. *Nature* 426, 353–359. <https://doi.org/10.1038/nature02135>
- Sloan, E.D., Koh, C.A., 2007. *Clathrate Hydrates of Natural Gases*. CRC Press.
- Sloan, E.D., Koh, C.A. 2008. *Clathrate Hydrates of Natural Gases*, third ed. CRC Press-Taylor & Francis Group, Boca Raton, Florida
- Smith, A.J., Mienert, J., Bünz, S., Greinert, J., 2014. Thermogenic methane injection via bubble transport into the upper Arctic Ocean from the hydrate-charged Vestnesa Ridge, Svalbard. *Geochemistry, Geophysics, Geosystems* 15, 1945–1959. <https://doi.org/10.1002/2013GC005179>
- Schmittner, A., Latif, M., Schneider, B., 2005. Model projections of the North Atlantic thermohaline circulation for the 21st century assessed by observations. *Geophysical Research Letters* 32. <https://doi.org/10.1029/2005GL024368>
- Somoza, L., Díaz-del-Río, V., León, R., Ivanov, M., Fernández-Puga, M.C., Gardner, J.M., Hernández-Molina, F.J., Pinheiro, L.M., Rodero, J., Lobato, A., Maestro, A., Vázquez, J.T., Medialdea, T., Fernández-Salas, L.M., 2003. Seabed morphology and hydrocarbon seepage in the Gulf of Cádiz mud volcano area: Acoustic imagery, multibeam and ultra-high resolution seismic data. *Marine Geology, Sedimentary Processes and Seafloor Hydrocarbon Emission on Deep European Continental Margins* 195, 153–176. [https://doi.org/10.1016/S0025-3227\(02\)00686-2](https://doi.org/10.1016/S0025-3227(02)00686-2)
- Stadnitskaia, A., Ivanov, M.K., Blinova, V., Kreulen, R., van Weering, T.C.E., 2006. Molecular and carbon isotopic variability of hydrocarbon gases from mud volcanoes in the Gulf of Cadiz, NE Atlantic. *Mar. Pet. Geol.* 23, 281–296.
- Sulpis, O., Boudreau, B. P., Mucci, A., Jenkins, C., Trossman, D. S., Arbic, B. K., & Key, R. M. 2018. Current CaCO₃ dissolution at the seafloor caused by anthropogenic CO₂. *Proceedings of the National Academy of Sciences*, 115(46), 11700-11705.



- Thomas, D.J., Zachos, J.C., Bralower, T.J., Thomas, E., Bohaty, S., 2002. Warming the fuel for the fire: Evidence for the thermal dissociation of methane hydrate during the Paleocene-Eocene thermal maximum. *Geology* 30, 1067–1070. [https://doi.org/10.1130/0091-7613\(2002\)030<1067:WTFFTF>2.0.CO;2](https://doi.org/10.1130/0091-7613(2002)030<1067:WTFFTF>2.0.CO;2)
- Tohidi, B., Yang, J., Salehabadi, M. et al., 2010. CO₂ hydrates could provide secondary safety factor in subsurface sequestration of CO₂. *Environmental science & technology*, vol. 44, pp. 1509–1514. <https://doi.org/10.1021/es902450j>
- Vadakkepuliyambatta, S., Chand, S., Bünz, S., 2017. The history and future trends of ocean warming-induced gas hydrate dissociation in the SW Barents Sea. *Geophysical Research Letters* 44, 835–844. <https://doi.org/10.1002/2016GL071841>
- Vassilev, A., Dimitrov, L., 2002. Spatial and quantity evaluation of the Black Sea gas hydrates. *Russian Geology and Geophysics* 43, 672–684.
- Vaular, E.N., Barth, T., Haffidason, H., 2010. The geochemical characteristics of the hydrate-bound gases from the Nyegga pockmark field, Norwegian Sea. *Organic Geochemistry* 41, 437–444. <https://doi.org/10.1016/j.orggeochem.2010.02.005>
- Vázquez, J.T., Palomino, D., Sánchez-Guillamón, O., Somoza, L., Fernández-Puga, M.C., Fernández-Salas, L.M., Medialdea, M., Fraile-Nuez, E., González, F.J., León, R., López-González, N., 2015. Geomorphological characteristics of the Passage of Lanzarote (East Canary Islands Region), in: Díaz-del-Río, V., Barcenas, P., Fernández-Salas, L.M., López-González, N., Palomino, D., Rueda, J.L., Sánchez-Guillamón, O., Vázquez, J.T. (Eds.), *Volumen de Comunicaciones Presentadas En El VIII Simposio Sobre El Margen Ibérico Atlántico*. Unpublished, pp. 575–578. <http://rgdoi.net/10.13140/RG.2.1.1699.3766>
- Vellinga, M., Wood, R.A., 2002. Global Climatic Impacts of a Collapse of the Atlantic Thermohaline Circulation. *Climatic Change* 54, 251–267. <https://doi.org/10.1023/A:1016168827653>
- Vogt, P.R., Cherkashev, G.A., Ginsburg, G.D., Ivanov, M.K., Crane, K., Lein, A., Sundvor, E., Pimenov, N., Egorov, A.V., 1997. Haakon Mosby Mud Volcano provides unusual example of venting - Vogt - 1997 - *Eos, Transactions American Geophysical Union - Wiley Online Library*. *Eos* 78.
- Waghorn, K.A., Bünz, S., Plaza-Faverola, A., Johnson, J.E., 2018. 3-D Seismic Investigation of a Gas Hydrate and Fluid Flow System on an Active Mid-Ocean Ridge; Svyatogor Ridge, Fram Strait. *Geochemistry, Geophysics, Geosystems* 19, 2325–2341. <https://doi.org/10.1029/2018GC007482>
- Woodside, J.M., Ivanov, M.K., Limonov, A.F., 1997. Neotectonics and fluid flow through the seafloor sediments in the Eastern Mediterranean and Black Seas. Part I: Eastern Mediterranean Sea. *IOC Technical Series* 48, 1–128.
- Yefremova, A.G., Zhizhchenko, B.P., 1974. Occurrence of crystal hydrates of gas in sediments of modern marine basins. *Doklady Akademii Nauk SSSR* 214, 1179–1181.
- You, K., Flemings, P.B., Malinverno, A., Collett, T.S., Darnell, K., 2019. Mechanisms of Methane Hydrate Formation in Geological Systems. *Reviews of Geophysics* 57, 1146–1196. <https://doi.org/10.1029/2018RG000638>
- Zander, T., Haeckel, M., Berndt, C., Chi, W.-C., Klaucke, I., Bialas, J., Klaeschen, D., Koch, S., Atgin, O., 2017. On the origin of multiple BSRs in the Danube deep-sea fan, Black Sea. *Earth and Planetary Science Letters* 462, 15–25. <https://doi.org/10.1016/j.epsl.2017.01.006>
- Wallmann, K., Pinero, E., Burwicz, E., Haeckel, M., Hensen, C., Dale, A., Ruepke, L., 2012. The Global Inventory of Methane Hydrate in Marine Sediments: A Theoretical Approach. *Energies* 5, 2449–2498. <https://doi.org/10.3390/en5072449>
- Wallmann, K., Riedel, M., Hong, W.L., Patton, H., Hubbard, A., Pape, T., Hsu, C.W., Schmidt, C., Johnson, J.E., Torres, M.E., Andreassen, K., Berndt, C., Bohrmann, G., 2018. Gas hydrate dissociation off Svalbard induced by isostatic rebound rather than global warming. *Nature Communications* 9, 83. <https://doi.org/10.1038/s41467-017-02550-9>
- Wessel, P., Smith, W.H.F., 1998. New, improved version of generic mapping tools released. *Eos, Transactions American Geophysical Union*, vol. 79, pp. 579–579. <https://doi.org/10.1029/98EO00426>
- Zitter, T.A.C., Huguen, C., Woodside, J.M., 2005. Geology of mud volcanoes in the eastern Mediterranean from combined sidescan sonar and submersible surveys. *Deep Sea Research Part I: Oceanographic Research Papers* 52, 457–475. <https://doi.org/10.1016/j.dsr.2004.10.005>